2005

The Effect of Red Blood Cell Velocity on Oxygenation Measurements using Resonance Raman Spectroscopy

Derrick Williams
Virginia Commonwealth University

EFFECT OF RED BLOOD CELL VELOCITY ON OXYGENATION MEASUREMENTS USING RESONANCE RAMAN SPECTROSCOPY

A thesis submitted in partial fulfillment of the requirements for the degree of Master of Science at the Medical College of Virginia Campus, Virginia Commonwealth University

by

Derrick Williams, B.S.
James Madison University, 2001

Advisor
Ivo P. Torres Filho, M.D., Ph.D
Associate Professor
Department of Anesthesiology
Department of Physiology

Virginia Commonwealth University
Richmond, Virginia
July, 2005

DEDICATION

To Angie for her steadfast love, support, and guidance.
She is my inspiration and my light.

ACKNOWLEDGEMENTS

I would like to thank my thesis advisor, Dr. Ivo Torres Filho for his constant support and guidance during this project. His complete willingness to accommodate my project, and its numerous time delays and mistakes, into his schedule under very limited time constraints was phenomenal and instrumental in allowing me to complete this thesis. I greatly appreciate his faith and trust in me to fully explore my project, its potential as well as its numerous complications.

I would also like to thank his wonderful wife, Dr. Luciana Torres for her surgical expertise and unflagging support and selflessness during the most stressful times of my project. Her tremendous help during the animal surgeries increased my efficiency tremendously. It is quite possible I would still be performing surgeries if it was not for her help.

I would like to extend my gratitude to the other members of my graduate committee, Dr. Wayne Barbee and Dr. Roland Pittman. Their patience and willingness to work with me under limited time constraints was greatly appreciated.

Thanks are also in order for Brian Ewbank, whose uncanny ability to locate blood for use in this project under very short notice was much appreciated. I also appreciate his support and conversation throughout the entire year I worked on this project. Leo Somera III also deserves acknowledgement for patiently teaching me how to use virtually all the equipment in the lab and making sure I didn't break anything in the process of learning how to use it on my own. His computer and general laboratory expertise was essential to my completing this project. The rest of my colleagues in the VCURES team deserve thanks for also supporting me throughout my project with great conversation, technical expertise in all aspects of the lab, and good humor.

I would like to thank my family for their unwavering love and support throughout not only my project but my academic career. I would not be where I am at this point without them. I cannot express in words how blessed I am to have them in my life. They mean the world to me.

TABLE OF CONTENTS

LIST OF TABLES

LIST OF FIGURES

Page

LIST OF ABBREVIATIONS

2,3 DPG	2, 3 diphosphoglyercate
A	available surface area
α	alpha
β	beta
CCD	charge coupled device
cm	centimeter
cm^{-1}	wavenumber
CO	carbon monoxide
CO_2	carbon dioxide
°C	Celsius
D	diffusion coefficient for oxygen
deoxy-Hb	deoxygenated hemoglobin
dL	deciliter
g	gram
Hb	hemoglobin
HbO_2	oxy-hemoglobin
Hb O_2 Sat	hemoglobin oxygen saturation
I_{oxy}	spectral intensity of resonance band for oxygenated hemoglobin
I_{deoxy}	spectral intensity of resonance band for deoxygenated hemoglobin
IR	infrared
IV	intravenous
kg	kilogram
λ_{inc}	incident light wavelength
λ_{scatt}	scattered light wavelength
met-Hb	methemoglobin
μm	micrometer
mg	milligram
min	minute
mL	milliliter
mm	millimeter
mmHg	millimeters of mercury
mW	milliwatt
nm	nanometer
N_2	nitrogen
ND	neutral density
O_2	oxygen
oxy-Hb	oxygenated hemoglobin
PCO_2	partial pressure of carbon dioxide
PE	polyethylene

π	pi
PO_2	partial pressure of oxygen
PR	peak ratio
Q	blood flow
sec	second
RBC	red blood cell
RR	resonance Raman
tHb	total hemoglobin concentration
UV	ultraviolet
Δx	diffusion distance

ABSTRACT

EFFECT OF RED BLOOD CELL VELOCITY ON OXYGENATION MEASUREMENTS USING RESONANCE RAMAN SPECTROSCOPY

By Derrick V. Williams, M.S.

A thesis submitted in partial fulfillment of the requirements for the degree of Master of Science at Virginia Commonwealth University

Virginia Commonwealth University, 2005

Director of Thesis: Ivo Torres Filho M.D., Ph.D
Associate Professor
Department of Anesthesiology

Resonance Raman spectroscopy can be used to estimate the hemoglobin oxygen saturation. Previous studies have demonstrated that exposure of oxygenated red blood cells to laser illumination may result in photo-induced displacement of oxygen from hemoglobin. In this study, an *in vitro* model was used to evaluate the relationship between this photo-induced effect and the red blood cell velocity. A computer-controlled system was implemented to acquire variables such as red cell velocity, microvessel diameter and hemoglobin oxygen saturation at multiple sites in selected microvascular networks. Using this system, resonance Raman spectroscopy was employed to measure hemoglobin oxygen saturation gradients in arterioles and venules of the rat mesentery *in vivo*. In several *in vitro* experimental conditions, there was a significant decrease in

photodamage as red cell velocity increased. As blood flowed downstream in arterioles and venules, increased red blood cell velocity was associated with smaller hemoglobin oxygen saturation gradients *in vivo*.

INTRODUCTION

Oxygen Transport in the Circulatory System

The circulatory system is composed of arteries, which carry oxygenated blood from the heart to the rest of the body, and veins, which carry deoxygenated blood back to the heart. The circuitry of this system is designed to deliver oxygenated blood from arteries into arterioles, smaller vessels composed of smooth muscle that can alter the size of the vessel lumen. In effect, arterioles act as resistance vessels, able to modulate blood flow throughout the circulatory system. Terminal arterioles branch into capillaries, microscopic, thin-walled vessels that form complex networks in tissue. The thin walls of the capillary, often only one cell layer thick, make it an ideal location within the vascular network to exchange diffusible substances between the blood and tissue. Once the blood has flowed through the capillaries it enters venules, which merge into veins to carry deoxygenated blood back to the heart (Levy 2004).

The blood that flows through the circulatory system is composed of red blood cells, white blood cells, and plasma, a complex aqueous medium that aids the transportation of these cells throughout the body. Although there are many important substances transported within the blood, gases such as oxygen (O_2) and carbon dioxide (CO_2) are vital to the minute-to-minute health of an organism. Red blood cells are the single element of blood responsible for the delivery of oxygen to all tissues and the

release of carbon dioxide, a waste byproduct of all fully functioning cells. All red blood cells contain the major oxygen carrier of the human body, a protein called hemoglobin (Hb). Ninety eight percent of all oxygen in the blood is carried by this protein, while the remaining 2% is carried in the plasma and red blood cell cytoplasm.

The hemoglobin protein is composed of two dissimilar pairs of polypeptide globin subunits – each globin subunit containing an alpha chain and a beta chain. Each globin subunit is attached covalently to a prosthetic heme group. Heme is comprised of a protoporphyrin cage surrounding an iron atom. Each iron within the heme can bind one oxygen molecule, so that a hemoglobin tetramer can bind up to four molecules of oxygen (Levy 2004). A unique, yet vital, property of hemoglobin is the ability to cooperatively bind oxygen. This means that the first oxygen molecule to bind to hemoglobin causes a conformational change in structure that facilitates the binding of O_2 at the other three binding sites. Conversely, release of O_2 by any of the iron atoms enhances the release of O_2 molecules from the remaining iron atoms. This property maximizes the amount of oxygen uptake in the lungs and delivery to the tissue.

Oxygen Delivery in the Blood

Oxygen delivery throughout the systemic circulation is dependent on reversible chemical reactions that are mediated by specialized compounds and catalysts. The pulmonary circulation brings blood in contact with specialized sacs in the lungs called alveoli where oxygen transfer from inspired air takes place. Passive diffusion transfers the oxygen from an area with a high oxygen partial pressure (PO_2) to deoxygenated blood

that has a substantially lower PO_2. This gradient helps drive the oxygen into the blood so that oxygenated blood can be distributed throughout the body (Levy 2004). Oxygen combines rapidly and reversibly with hemoglobin to form oxy-hemoglobin (HbO_2). Hemoglobin that is not combined with O_2 is called deoxy-hemoglobin.

The amount of O_2 chemically combined with hemoglobin depends on the PO_2 in the blood. Arterial PO_2 is not normally high to fully saturate all the Hb with O_2. The amount of O_2 actually bound is often less than capacity, thus, the term hemoglobin oxygen saturation (Hb O_2 Sat) is used to describe the ratio of hemoglobin-bound oxygen to the maximal amount of O_2 that can bind. An increase in PO_2 leads to an increase of oxygen saturation. This relationship, expressed graphically as the Hb O_2 dissociation curve, is sigmoidal, rather than linear. This curve shows a relatively wide range of near constant oxygen saturations at PO_2 levels above 70-80 mmHg. However, at low PO_2 levels (below 40 mmHg) the changes in saturation are more pronounced. This property of hemoglobin dissociation allows for the satisfaction of increased metabolic demands for O_2 with small reductions in tissue PO_2 (Levy 2004; Levy 2004).

There are several factors that can affect the amount of O_2 bound to hemoglobin, namely, the partial pressure of CO_2 (PCO_2), pH, blood temperature, and 2,3 diphosphoglycerate (2, 3 DPG), a metabolic intermediate formed by red blood cells. The Hb O_2 dissociation curve is shifted to the right by an increase in temperature, PCO_2, or 2, 3 DPG. A similar shift can be caused by a decrease in pH. This shift is termed the Bohr shift and indicates that at any given partial pressure of O_2 under these conditions, hemoglobin is less saturated with oxygen. These conditions are often an indicator of increased oxygen demand by the tissues. The Bohr shift allows more oxygen to be bound

to hemoglobin in the lungs at a lower PO_2, where these conditions are not prominent. When oxygenated blood reaches the tissues with increased oxygen demand, more oxygen is released at a given PO_2 (Levy 2004).

Microcirculatory Oxygenation and O_2 Distribution

The microcirculation refers to the microvessels that play the central role in delivering oxygen to tissue. These microvessels include arterioles, capillaries, and venules. Oxygen is moved throughout these vessels using two processes, convection and diffusion. Convection refers to the flow of blood through the circulatory system and is an effective method of delivering large amounts of oxygen over significant distances. Diffusion is the random movement of molecules, from regions of high PO_2 to low PO_2 driven by partial pressure. In the case of oxygen, diffusion is the primary method of oxygen transport over the distance of tens of microns, a distance seen exclusively in the thin walls of capillaries. This diffusion is driven by the difference in partial pressure of oxygen across the capillary wall. The rate of diffusion is described by Fick's Law:

$$\text{Rate of Diffusion} = D\alpha A\,(PO_2/\Delta x)$$

Where D is the diffusion coefficient of oxygen, α is the solubility of oxygen, A is the available surface area for oxygen exchange, PO_2 is the partial pressure difference across the capillary wall, and Δx is the distance that the oxygen travels to its destination in the tissue (Pittman 1998).

Pioneering work by August Krogh in the 1920's strongly suggested that the primary vascular site for oxygen transport from blood to tissue was the capillary network.

Capillaries appeared to be ideal sites for gas exchange due to their thin walls, large surface area-to-volume ratio, low RBC velocity, and short diffusion distances (Krogh 1959). However, later studies directly measuring oxygen tension within and outside arterioles demonstrated a progressive fall in oxygen tension from the largest arterioles to the terminal arterioles (Duling and Berne 1970). Recent studies have shown a decreasing longitudinal PO_2 gradient as blood moves downstream in the arteriolar network (Intaglietta, Johnson et al. 1996; Torres Filho, Kerger et al. 1996; Tsai, Johnson et al. 2003). This supported the idea of oxygen release from precapillary microvessels.

Several studies have examined the longitudinal hemoglobin oxygen saturation gradient in a variety of microvessels in locations such as striated muscle and the retina. In the pial vessels of the rat, an estimated 21% of the oxygen present in the arterial circulation was lost before entering the capillary network (Ivanov, Derry et al. 1982). A significant gradient of arteriolar oxygen tension was observed in the retinal vessels of the cat which revealed a 2.5 – 4.0 mmHg decrease over only 500 μm (Tsai, Johnson et al. 2003). Work by Swain and Pittman demonstrated a decrease in Hb O_2 Sat from first order arterioles, indicated by having diameters of approximately 60 μm, to fourth order arterioles, which are notably narrower. An Hb O_2 Sat decrease from 71% in these large microvessels to 60% in smaller vessels was observed. The calculated Hb O_2 Sat gradient indicated an average decrease of 2%/mm in 1st order arterioles to 18%/mm in 4th order arterioles (Swain and Pittman 1989). In this same study, it was found that venular gradients tended to be distributed such that microvessels with high Hb O_2 Sat had high flow rates and those with low Hb O_2 Sat had low flow rates. Longitudinal hemoglobin saturation gradients within terminal arterioles were positively correlated with blood flow.

Additionally, these gradients also were largest in these microvessels, despite having the shortest distance for oxygen exchange.

Due to the permeable nature of virtually all vessels of the microcirculation, oxygen distribution is very complex due to the close proximity of numerous capillaries, arterioles, and venules to each other. Oxygen transfer can occur between precapillary vessels, tissues, and postcapillary vessels without contact with capillaries themselves. Arrangements that bring arterioles and venules in close proximity have been shown to increase oxygen transfer from the arteriole into the venule (Kobayashi and Takizawa 2002). In this study, Hb O_2 Sat levels in venules increased after crossing arterioles with higher Hb O_2 Sat levels. Hb O_2 Sat levels in arterioles decreased after crossing venules with lower Hb O_2 Sat levels, indicating oxygen transfer via diffusion. Studies of the microvasculature in the rat mesentery have revealed a distinct decrease in PO_2 as blood flowed through the microvessels longitudinally (along the axis of flow) and radially (perpendicular to this axis) (Itoh, Yaegashi et al. 1994).

Noninvasive Measurement of Oxygen Content

Although there are numerous methods of measuring the oxygen content of blood and tissue, almost all of them require either removal of the tissue or collection of blood. This limits the amount of further analysis of the given tissue and prevents *in vivo* measurement of microvascular parameters such as PO_2, hematocrit, and Hb O_2 Sat. Optical measurements of oxygen distribution within the microvasculature assess the levels of the two interrelated indicators of oxygen content, PO_2 and Hb O_2 Sat.

Noninvasive measurement of these microvascular parameters *in vivo* is ideal because it avoids perturbation of the blood and tissue. The development of the techniques that allow for the optical measurement of hemoglobin oxygen saturation will be outlined below.

There are two primary methods of noninvasively measuring Hb O_2 Sat in the blood aside from clinical oximetry: the 3-wavelength method and the resonance Raman spectroscopy method (Torres Filho, Terner et al. 2005). The details of the three wavelength method have been previously described (Pittman and Duling 1975; Pittman 1986) so only a very brief summary will be provided here. This method takes advantage of the light absorption properties of blood, depending on its oxygenation state. Essentially, it measures the optical densities of blood at three different wavelengths while correcting for the estimated nonspecific light losses in the system. This method was been demonstrated to be extremely accurate at a wide range of i*n vivo* conditions.

The technique of resonance Raman spectroscopy has been recently published (Torres Filho, Terner et al. 2005). This method utilized the previously described 3-wavelength method to confirm an alternative optical method of measuring hemoglobin oxygen saturation that can detect the oxy and deoxy forms of hemoglobin. A comparison of the ratio of the two forms allows for a calculation of the estimated hemoglobin oxygen saturation. A detailed explanation of the theory behind this technique is described below.

Vibrational Spectroscopy

The basis for this technique is the unique interaction between light and matter, known as the Raman effect. When light strikes a substance, the photons can be scattered or absorbed. When the photons are scattered, most of the scattered light and incident light will have the same frequency. However, a small fraction of the incident light can transfer its energy to the molecules of the substance, setting it into vibration. Since light energy is proportional to frequency, the frequency change of the scattered light must equal the vibrational frequency of the scattered molecules. This energy exchange describes the Raman effect (Hanlon, Manoharan et al. 2000). The energy transition may be translational, rotational, vibrational, or electronic in nature (Spiro 1974).

The process of simultaneous absorption of an incident photon and emission of a Raman scattered photon can be captured using a spectrometer and a detector. The detector can capture the scattered photons created during this process and display the intensity of the scattered light as a function of the frequency shift. This frequency shift is commonly referred to as the Raman shift, defined by the equation:

$$\text{Raman shift} = 1/\lambda_{inc} - 1/\lambda_{scatt},$$

where λ_{inc} and λ_{scatt} are the incident and Raman scattered light wavelengths (in cm), respectively (Wang and Van Wart 1993). The frequency shifts depicted in a Raman spectrum are traditionally measured in wavenumbers (cm^{-1}), a unit that relates the energy of the scattering molecule to change in frequency of the scattered light.

Resonance Raman (RR) Spectroscopy

Resonance enhancement of Raman bands occurs when the incident light energy approaches that of an absorption band region. If the excitation light occurs within this band, more of the incident energy is transferred, resulting in a more dramatic frequency shift in the scattered photons. This coupling enhances the intensity of the Raman signal (Spiro and Czernuszewicz 1995). Fluorescence produces a broad spectral band that can easily obscure resonance Raman spectra (Spiro 1974). If fluorescence can be reduced, resonance enhancement can greatly intensify the Raman spectra of the vibrational Raman scattering processes.

Vibrational spectroscopy, available from Raman spectra, allows for the measurement of vibrational frequencies, which are sensitive to geometric and bonding arrangements of localized groups of atoms (Spiro 1974). Biological molecules, such as cholesterol and hemoglobin, can be analyzed for the vibrations of groups of atoms within them (Spiro 1974; Hanlon, Manoharan et al. 2000). As described previously, RR spectroscopy allows for the selective enhancement of Raman scattering within a particular electronic absorption band. Many RR bands are not affected by this absorption, but others may be enhanced greatly. This effect is caused by a coupling of electronic and vibrational transitions, which tend to be localized on atom groups called chromophores. Chromophores include heme, flavins, and metal ions and tend to be located at sites within the macromolecule that have biological function. Resonance Raman spectroscopy allows for a monitoring of atoms at these biologically active sites with little interference from the rest of the atoms within a given molecule (Spiro 1974).

The resonance Raman phenomenon can be created using several excitation methods. Ultraviolet (UV), visible, and near infrared (IR) lasers can be used to excite a given molecule. UV resonance excitation is advantageous because it causes the most excited molecular vibrational state of the three methods. The fluorescence caused by UV excitation is shifted to lower frequences than the Raman scattered light frequency, further increasing the resolution of UV-induced resonance Raman scattering. The difficulty in using visible excitation results from frequencies of the fluorescent and Raman scattered light being very similar. This leads to intense fluorescence that can obscure the Raman spectra (Hanlon, Manoharan et al. 2000). Near IR excitation may also be as effective as UV excitation because this light is too low a frequency to excite significant fluorescence.

Heme Scattering and Oxygenation State of Hemoglobin

The ability of RR spectroscopy to examine the unique vibrational state of chromophores can be used to determine the oxygenation state of hemoglobin. As described previously, this oxygen carrier protein is responsible for binding the individual O_2 molecules in red blood cells (RBC's). The specific chromophore responsible for binding oxygen, heme, has been shown in several studies to demonstrate very clear resonance Raman spectra (Spiro and Strekas 1974; Wood, Tait et al. 2001). The presence of visible (α and β) or near UV (Soret) Raman bands cause this resonance excitation at wavenumbers between 1000 and 1700 cm^{-1}. Within each of these bands, excitation wavelength in the vicinity of either visible or near UV spectra will reveal more specific Raman bands (Spiro 1974). The iron porphyrin complex of heme exhibits distinct

resonance Raman spectra depending on the oxygenation state. Near UV excitation of heme proteins will cause a strong resonance Raman enhancement in the 1350 – 1380 cm^{-1} range. The Raman spectra of this enhancement will be slightly different, depending on the oxidation state of the iron molecule within heme (Spiro and Strekas 1974).

The term deoxy-hemoglobin describes hemoglobin in which the iron bound within the heme protein is reduced. Near UV excitation of this oxygenation configuration as been demonstrated to display a strong Raman band at 1357 cm^{-1}. Oxy-hemoglobin refers to hemoglobin in which the iron molecule is oxidized. Similar excitement of this state has shown a strong Raman band at 1376 cm^{-1} (Wood 2002).

Photo Effects of Laser Excitation

Usage of a laser to provide the excitation light necessary to create a resonance Raman spectrum has been demonstrated to cause hemolysis and cell damage in living samples (Puppels, Olminkhof et al. 1991; Wood 2002). Hemoglobin, in particular, can be converted from oxy-hemoglobin to deoxy-hemoglobin when constantly exposed to light of varying electromagnetic spectra such as UV, visible, or near IR. It has been shown that a light-induced deoxygenation process can be created in fully oxygenated hemoglobin by exciting a single RBC using lasers with total power above 2 mW. It was found that the extent of this photo-disassociation increased if the laser power was increased (Nollmann and Etchegoin 2000). Studies that have examined the effect of visible and near IR excitation on the Raman spectra of hemoglobin have revealed that the wavelength of excitation light is vital in eliminating the cell degradation and various photo-induced effects on hemoglobin (Wood 2002; Wood 2002). Excitation of living

cells with a 488-515 nm wavelength of light has been demonstrated to cause cell degradation. However, this effect was eliminated by using laser light of 632 or 660 nm (Puppels, Olminkhof et al. 1991).

Recent studies using single red blood cells have further clarified the mechanism of photo-damage. Constant exposure of a single fully oxygenated RBC to an excitation laser indicates that a small amount of the oxy-hemoglobin is converted to methemoglobin, an inactive form of the protein in which oxygen cannot bind. The rest of the oxy-hemoglobin is reversibly converted to deoxy-hemoglobin. Two other effects have been observed in this situation, using 514.5 nm excitation (3.2 mW): 1) a decrease in the intensity of both oxy and deoxy RR peaks ; and 2) an increase in fluorescence intensity (Ramser, Bjerneld et al. 2003). In a follow-up study, these authors used excitation lasers (0.75 mW) at three wavelengths: 488 nm, 514.5 nm, and 568.2 nm to generate RR spectra in single red blood cells. They found that there was less photo-disassociation of O_2 from the 568.2 nm excitation laser as compared to the 488 nm laser (Ramser, Logg et al. 2004).

Hemoglobin Oxygen Saturation Measurements Using Raman Spectroscopy

There is only one published study that has attempted to use resonance Raman spectroscopy to determine the Hb O_2 Sat of flowing blood *in vivo* (Torres Filho, Terner et al. 2005;). Using a correction factor in the calculation of the relative heights of the oxy and deoxy hemoglobin Raman peaks allows for an estimation of Hb O_2 Sat. This calculation was supported by measurement of hemoglobin oxygen saturation using the 3-

wavelength method. A good correlation was found between the calculated and measured values of Hb O_2 Sat (Torres Filho, Terner et al. 2005). Photo-induced effects were minimized by using very low laser energy (<0.3 mW) and examining flowing blood. Additionally, laser illumination time was reduced to 20-30 sec. Observations of unmoving blood, obtained *in vitro*, revealed a gradual decrease in intensity of HbO_2 peaks with a concomitant increase in deoxy Hb peak intensity under constant laser exposure and oxygen gas influx (Torres Filho et al., unpublished observations).

Multiple Site Microcirculatory Measurements

Few studies have developed methodologies to acquire multiple site microcirculatory measurements repeatedly. This type of data acquisition requires a certain degree of automation and motorized stage control often afforded by a specialized computer program. The development of numerous optical methods to make microcirculatory measurements have recently allowed for an extensive use of computer technology such that rapid data acquisition of these parameters was possible with a certain degree of automation. It has been demonstrated that computer controlled stages can allow for fast measurement of microvascular parameters such as RBC velocity, hematocrit, tissue and blood PO_2, and Hb O_2 Sat at multiple sites (Toth, Tischler et al. 1992; Pal, Toth et al. 1993). Further automation has allowed real time data analysis so that changes in the entire vascular network architecture and composition can be observed virtually as they occur *in vivo* (Bakker-Schut 2002).

Purpose of This Study

There were three main aims of this study. The first was to further explore the relationship between photo-disassociation of O_2 from hemoglobin and RBC velocity using near UV excitation in an *in vitro* environment. A determination was made of the approximate RBC velocity needed to reduce or eliminate photo-induced deoxygenation of oxy-hemoglobin using constant laser power. The second goal of this study was to implement a computer-controlled system to acquire variables such as red blood cell velocity, microvessel diameter, and hemoglobin oxygen saturation at multiple sites in selected microvascular networks. The last aim of this study was to use this system to measure hemoglobin oxygen saturation gradients in the arterioles and venules of microcirculatory networks using resonance Raman spectroscopy.

METHODS

Raman Intravital Microscope

The Raman intravital microscope used to capture Raman spectra in both *in vitro* and *in vivo* experiments is identical to that used by Torres Filho et al. (2005). It is an upright microscope (Axioplan Imaging 2, Zeiss, Thornwood, NY) adapted for resonance Raman spectroscopy using laser excitation. The preparation could be viewed using 20X and 40X water immersion objectives, with numerical apertures of 0.45 and 0.80, respectively (Zeiss, Thornwood, NY). All Raman spectra reported were obtained using the 40X water immersion objective.

The laser excitation was provided by a 406 nm external cavity semiconductor tunable continuous wave laser (TEC 100; Sacher Lasertechnik, Germany) connected to a controller (MLD-1000; Sacher Lasertechnik, Germany) that allowed for an adjustment of the laser intensity. The laser beam was directed by a mirror onto the epi-illumination optical path of the microscope. The presence of a band pass filter and two pinholes placed in the optical path removed the plasma emission lines from the laser beam. The laser light was reflected onto the preparation via a 2 mm mirror mounted inside the microscope. Using the 40 X objective, the laser light spot had a diameter of 15-25 μm, measured at the focal plane. The backscattered light from the sample was collected by the objective and directed back into the microscope along the same path as the incident laser beam. The scattered Raman light of the desired range (greater than 420 nm) was

collected by an attenuation of the Rayleigh line via a high quality long pass filter. The Raman light emitted from the sample was projected through the entrance slit of the spectrometer (SpectraPro, Acton Research Co., Acton, MA). This slit was adjusted, via a mechanical adapter, to an aperture of 20-30 μm to maximize light acquisition while preserving the definition in the oxy and deoxy peaks of the Raman spectra. A lens then recollimated this light and directed it onto the diffraction grating (2400 grooves/mm) of a mirrored prism. The diffracted light was directed by the second mirrored face of the prism to a 150 mm focal length lens that focused the light on to the detector. A back illuminated CCD detector (Spec10: 400B, Princeton Instruments, Trenton, NJ), cooled to -41.5 °C to reduce thermal noise, collected the Raman spectra at the desired wavelength range (above 420 nm). The detector was connected to a controller interfaced to a personal computer, where the spectra were collected using specialized software (Winspec, Princeton Instruments, Trenton, NJ). All collected Raman spectra were stored for future analysis. A schematic representation of this setup is depicted in Figure 1.

In vitro Circulator

In order to perform hemoglobin oxygen saturation (Hb O_2 Sat) measurements of blood under controlled conditions of temperature, velocity and oxygenation, a closed-circuit of tubing was constructed. A diagram of the setup is shown in Figure 2. A fluid circulator was created to circulate blood thought a flat 40 mm length of capillary tube with the following dimensions: 2 mm × 4 mm × 0.2 mm (reported in terms of internal

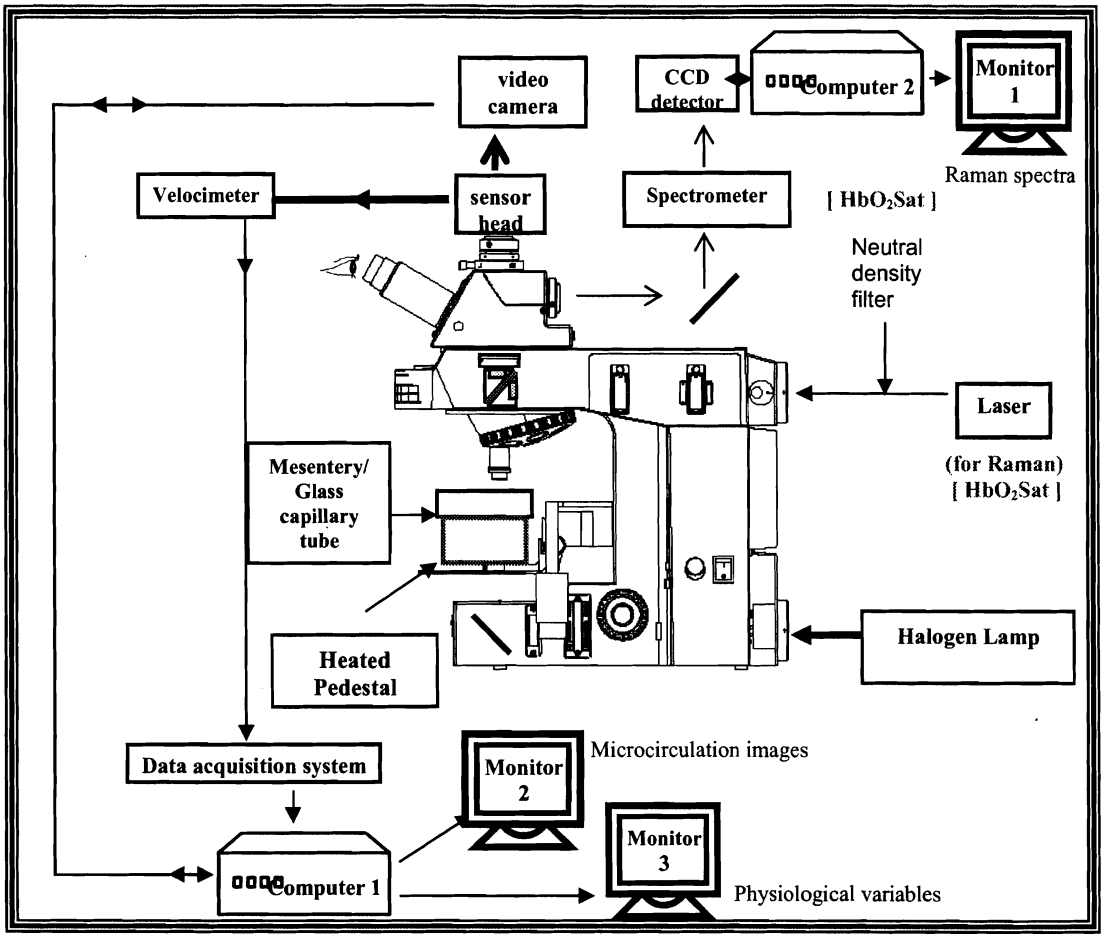

Figure 1. A diagram of the intravital microscopy system used to obtain microcirculatory parameters in this study.

Both trans- and epi-illumination paths can be activated simultaneously, allowing a visualization of the laser spot in dim halogen light. Thicker arrows indicate the transillumination path. Epi-illumination is indicated with thinner arrows. The data acquisition system also receives input from pressure transducer connected to the animal's arterial circulation. Modified from Figure 1 in Torres Filho et al. (2005)

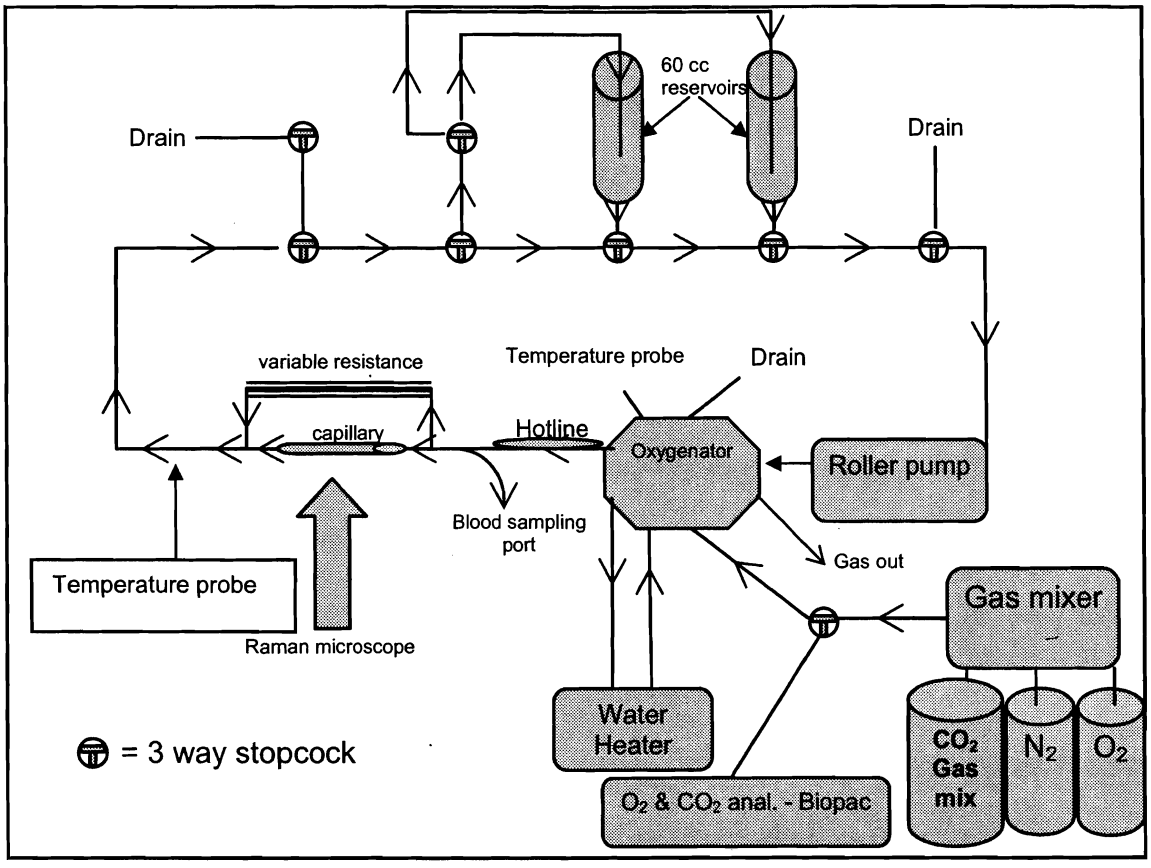

Figure 2. A schematic diagram of the *in vitro* circulator.

Arrows indicate the direction of blood flow. Blood was introduced into circulation via the 60 mL reservoirs. The RBC velocity through the capillary tube was adjusted by changing the resistance of the flow through the other fork of the main tubing line or by way of the roller pump.

height, internal width, and wall thickness, respectively). To adapt the ends to allow for circular tube attachment, they were heated with a Bunsen burner and stretched. This adaptation allowed small rubber tubing to be attached to the ends of the capillary tube, interfacing it with the rest of the circulating system. A peristaltic pump (Maserflex 7518-00, Cole-Parmer, Vernon Hills, IL) moved blood through a hollow fiber oxygenator (Capiox RX-05, Terumo Cardiovascular Systems; Ann Arbor, MI) that allowed for gas exchange with a mixture of nitrogen, oxygen, and CO_2. The circulating blood was also heated to 41 °C as it exited the oxygenator, as measured by a thermocouple (YSI; Yellow Springs, Ohio) exposed to the blood as it flowed. As the blood exited the oxygenator, it moved through 60 cm of plastic tubing encased in a hotline, a larger plastic tube enveloping the blood line that carried 45 °C water countercurrent to the movement of blood. This helped to keep the circulating blood warm enough to counteract the loss in temperature as it left the heated oxygenator. The blood then entered a virtually airtight cylindrical chamber adapted from an intravenous (IV) tubing set. This chamber acted as a dampener to maintain constant blood movement at very low RBC velocities (between 0.2 and 0.4 mm/sec). Polyethylene tubing carried the blood to a fork that routed it either through the capillary tube that allowed for viewing under a microscope or through plastic tubing of the same dimensions as the rest of the system. This tubing network was affixed to a Plexiglass platform using hot glue. A plastic clamp was used adjust the velocity of the blood through the capillary side of the fork by varying the resistance through the main blood line. Once the blood crossed the capillary tube, it rejoined the main blood flow and exited the platform. A second thermocouple measured the temperature just before the blood exited the platform. In all experimental conditions, the temperature of the blood as

it exited the platform was maintained between 35.5 and 37 °C. Upon exit, the blood was returned to a 60 mL syringe reservoir, the beginning of the circulation loop. A circulating water bath circulator (DC10, Thermo-hake, Newington, NH) provided the heated water used to heat the hotline and oxygenator. Blood was drawn using a length of PE-20 tubing that allowed for samples (0.06 ml) to be taken a distance of 25 mm from the entrance to the capillary tube.

In vitro Circulator Preparation

To prepare the circulator for the *in vitro* experiments, it was cleaned by circulating a large volume of diluted enzymatic cleaning solution (Maxizyme, Henry Schein, Inc, Melville, NY) until the reservoir filled with fluid the same color as the cleaning solution. After the system was completely drained, 60 mL of heparin solution (10 units/mL of normal saline) was circulated through the system for 5 minutes. This solution was subsequently drained and 80 mL of pig blood (obtained using sterile technique from the carotid artery) was introduced into the system and allowed to warm to 36-37 °C for 5 minutes. Three separate gas tanks, containing 100 % N_2, 100 % O_2, and a gas mixture of 50 % O_2, 44 % N_2, and 6 % CO_2 respectively, were combined using two separate gas mixers (Aalborg Instruments, Orangeburg, NY) The resultant gas mixture was analyzed for the composition of oxygen and carbon dioxide using a sampling apparatus (O_2 sensor: model 201C-128 and CO_2 sensor: model 205C – 124, Biopac Systems, Goleta, CA) connected to a computer based data acquisition program (AcqKnowledge 3.8, Biopac Systems). This gas mixture was monitored to provide an

estimate of the oxygen and carbon dioxide levels as it entered the circulating blood through the oxygenator.

Two separate blood samples (0.06 mL) were collected, via the sampling line, 1-2 minutes after introduction of the gas mixture. They were drawn into heparinized micro-hematocrit capillary tubes (VWR Scientific Inc., Westchester, PA) for blood gas analysis and hematocrit determination. One sample was analyzed for Hb O_2 Sat, methemoglobin, and total hemoglobin concentration (tHb) using a CO oximeter (OSM3; Radiometer, Copenhagen, Denmark). The oximeter allowed adjustments for pig or rat blood, as needed. The other sample was placed in a centrifuge and spun to determine the hematocrit. Once a baseline Hb O_2 Sat and hematocrit were established, the Plexiglass platform was mounted on the stage of an upright microscope adapted (Axioplan Imaging 2, Zeiss) for resonance Raman spectroscopy using laser excitation.

Red Blood Cell (RBC) Velocity Measurement

RBC velocity measurements were obtained via a trans-illumination path of the microscope, using an optical Doppler velocimeter (Texas A&M University, College Station, TX). This is a well-established method that has been used in several previous studies (Borders and Granger 1984); (Davis 1987). It gives an average RBC velocity that can be digitally displayed or output to a data acquisition system that would allow for a more precise estimation of velocity. All RBC velocities reported were collected using the data acquisition system. Measurements were obtained by displaying the image of the red blood cells on one computer monitor. Once the image of the flowing blood was brought in focus, it was aligned between two black dots that mark the axis of measurement of the

velocimeter. Care was taken to optimize the RBC velocity measurement of blood flow by adjusting the axis of the flow between the two black dots. RBC velocity was calculated by taking a 5 second average of the resultant waveform. In all RBC velocity measurements, approximately 10-15 seconds of observation time was given to assure a stable velocity.

In vitro Data Collection

A Raman spectrum was obtained for the blood moving through the capillary tube only. Two to three spectra were obtained at each RBC velocity, within a range of 0.2 – 1.9 mm/sec. A 0.06 ml sample of blood was withdrawn from the system for OSM3 analysis of Hb O_2 Sat, methemoglobin, and tHb. Samples were withdrawn for analysis after every set of Raman spectra. RBC velocities were increased in a range of increments ranging from 0.1 to approximately 0.8 mm/sec. All Raman spectra were taken with accumulation times ranging from 5 to 20 seconds. The second phase of the experiment was to repeat the first phase but with a neutral density filter (ND 1.4) in place to reduce the laser power on the blood. The third, and final, phase of the experiment was a repeat of phase one but using a neutral density filter with higher optical density (ND 2.0). Due to the dramatically decreased light transmission through this filter, the accumulation time was increased to a minimum of 10 seconds but no longer than 20 seconds. This assured that all Raman spectra showed distinct oxy- and deoxy- hemoglobin peaks, allowing for future spectra analysis. Before the day of the experiment, the power of the incident laser to be used in all unfiltered experimental conditions to be tested was measured. The power measurement was made using the 40X objective focal point with a power meter (PD300-TP; Ophir Optronics, Wilmington, MA). The laser power of all filtered

conditions was calculated after the experiment by reducing the measured unfiltered laser power by the light reducing factor of the neutral density filter.

In vivo Procedure and Mesentery Preparation

Five to seven week old male Sprague-Dawley rats (n = 6, body weight = 341.5 g ± 16.2) were fasted overnight. They were anesthetized (at concentrations of 5 % and 2 %, induction and maintenance concentrations respectively) with Isoflurane (Baxter Pharmaceuticals, Deerfield, IL), followed by a constant intravenous infusion (0.39 – 0.58 $mg \cdot kg^{-1} \cdot min^{-1}$) of alfaxalone/alfadolone acetate (Saffan, Schering-Plough Animal Health, Welwyn Garden City, England). The core temperature of the animal was maintained with a homeothermic blanket (Harvard Apparatus, Holliston, MA). The trachea of the animal was cannulated with polyethylene tubing (PE-240) to ensure a patent airway throughout the experiment. The right jugular vein was cannulated with PE-50 polyethylene tubing for the administration of Saffan. The left carotid arterty was cannulated (PE-20) to monitor arterial blood pressure. Using a small, 25 mm long incision down the midline, cotton swaps soaked in warm saline were used to carefully exteriorize a section of ileal loop and associated mesentery. This section was gently placed on a Plexiglass viewing platform warmed to a surface temperature of 37 °C (Golub and Pittman 2003). After exposure, the preparation was covered with a thin plastic film (Saran Wrap, Dow Corning, Midland, MI) to reduce desiccation of the tissue and gas exchange with the atmosphere.

Computerized Stage Movement Program

In order to rapidly acquire Raman spectra and velocity measurements at various positions (x, y coordinates and focus) within a particular microcirculatory network in the rat mesentery, a customized stage movement script was written in IPLab (Scanalytics Inc, Fairfax, VA), a Windows-based computer program that automates many microscope functions. This program is unique in that it allows for many of these functions to be automated via a programmable interface called a script. One feature of IPLab is the ability to move the microscope stage and the focus knob, which are equipped with stepper motors. The electrical signals for the stepper motors are provided by motor drivers. These drivers receive commands from the IPLab computer via custom designed parallel I/O board containing an analog/digital converter unit. The precise movement of the stage can be controlled either by the computer using arrow keys or a joystick connected to an input port on the computer. The movement resolution can be set to either 0.1 or 1 μm/step in x, y, and z axis. IPLab uses an X-Y coordinate system with arbitrary units based on counting the step signals received by the stepper motors in a given direction. The range in both directions is -99999 to 99999 steps, corresponding to 8.3 cm of stage movement. This is similar to a stage movement system used in a study designed to rapidly capture stage positions for microcirculatory measurements (Pal, Toth et al. 1993).

In order to rapidly and accurately capture positions along the arterioles and venules of the microvascular network, a script was created to move the microscope stage to saved positions as indicated by the user. The script prompted the user to select the number of positions to be saved to a position table stored within IPLab. Additionally, the

user input the exposure time of the high resolution digital video camera (Coolsnap cf, Photometrics, Tucson, AZ) used for image capture. This allowed the light intensity reaching the camera to be regulated to prevent oversaturation of the display pixels on the computer screen. After this prompt, the camera was activated and the mesentery image could be viewed on one of the computer monitors. The user could now use the joystick to move the stage to the precise position along the network to be examined. The position would not be saved until the user pressed a button on the keyboard. This second prompt allowed all other measurements, such as 40X image acquisition and RBC velocity, to be taken. All positions along the network were captured in this manner. Once these positions were captured, the user was prompted to revisit these positions again in a second loop. The script was designed to continue to allow all saved points to be revisited in sequence indefinitely unless otherwise indicated by the user. A flow chart of the script and the actual script written are provided in Figure 3 & Figure 4, respectively.

In vivo Data Collection

The animal platform was positioned on the microscope stage and the mesenteric tissue was visualized under 20X water immersion objective. At this time, any microvascular networks were identified. These networks were only included in this study if a clear arteriole, capillary, and venule could be visualized. Four to six positions were identified along each network to be mapped (2-3 arteriolar points and 2-3 venular points). Positions were chosen that remained relatively immobile and were wide enough to allow for maximum laser spot contact, even if the preparation moved in the middle of a Raman capture. A paper sketch was created in which positions to be saved along the network

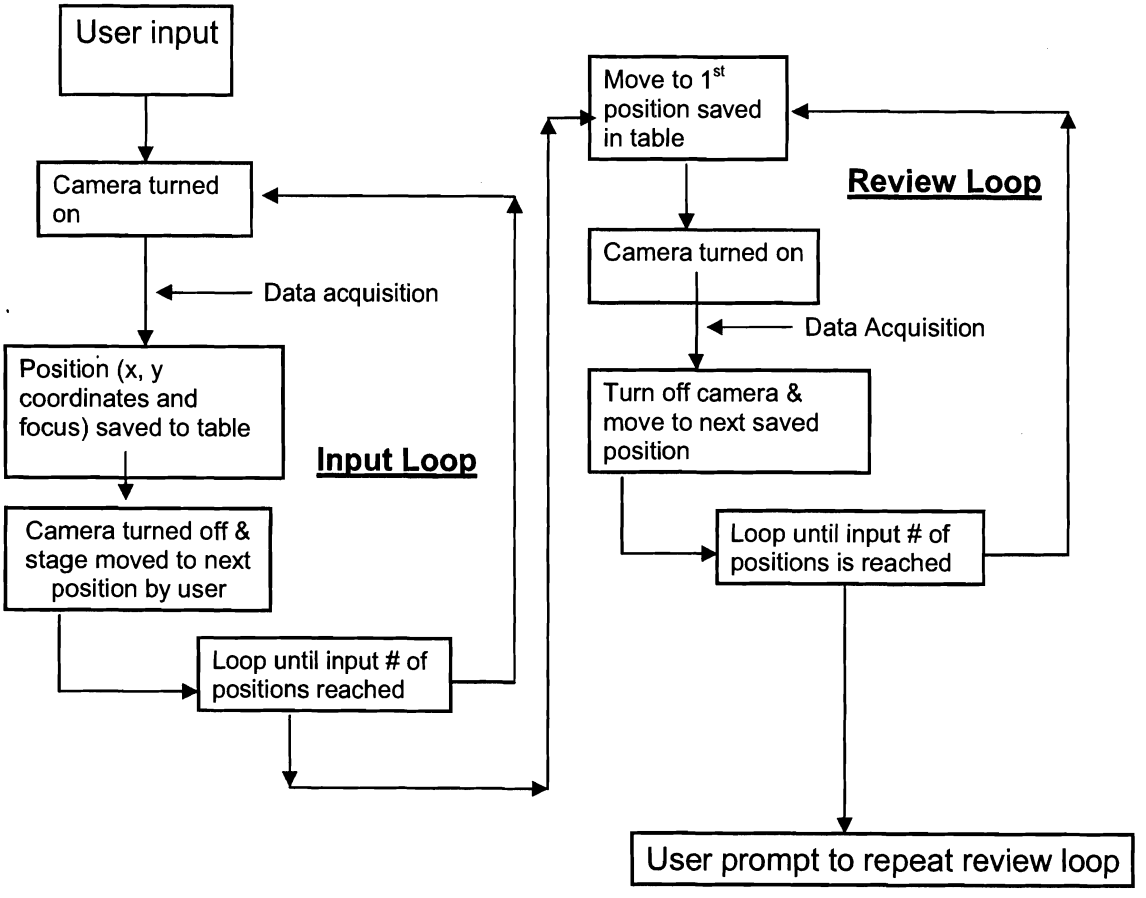

Figure 3. Flow chart of the IPLab stage movement script.

Data acquisition refers to any combination of diameter measurements, RBC velocity measurements, and Raman spectrum acquisition.

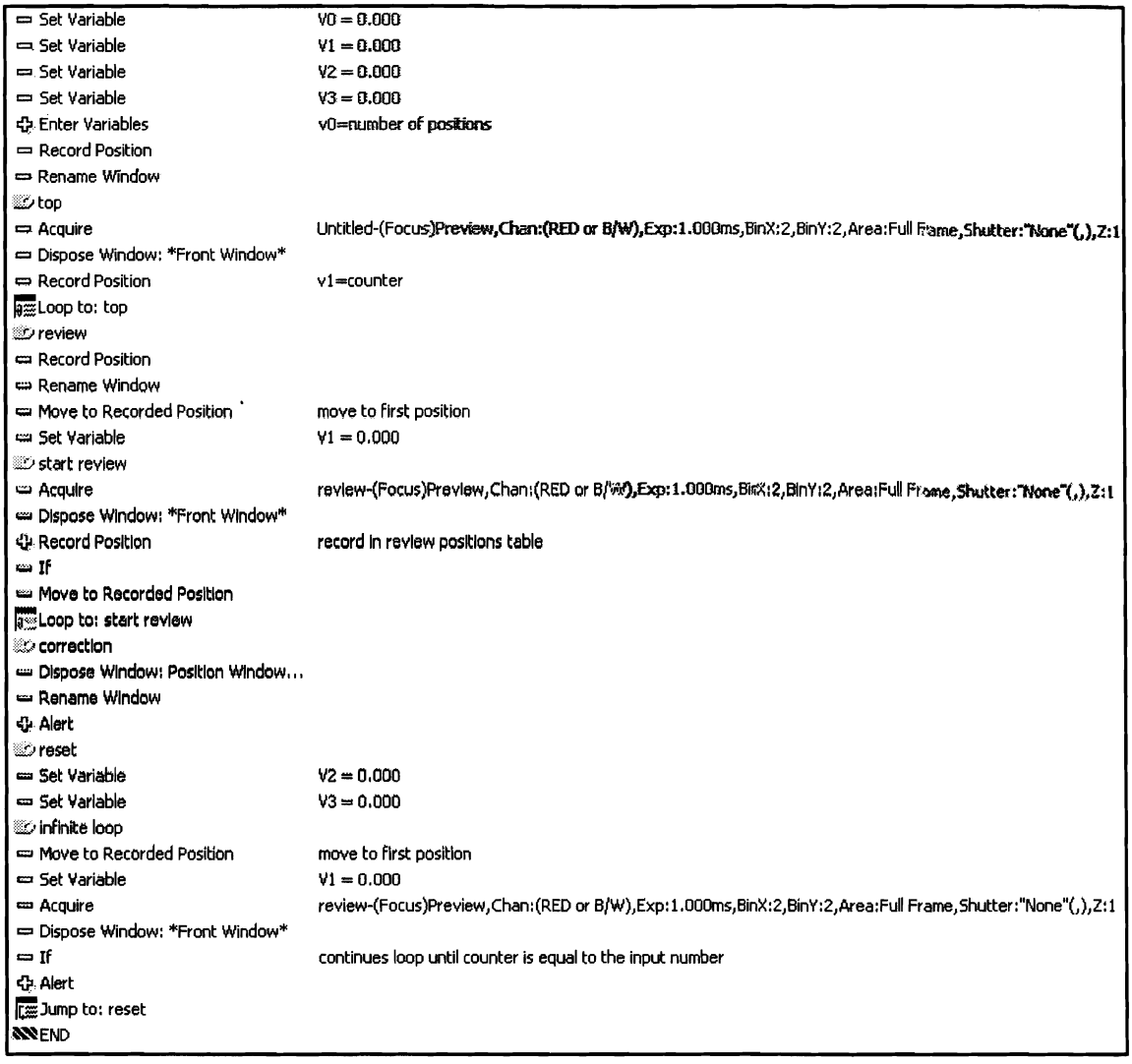

Figure 4. Actual IPLab script (software code) developed to record the X,Y coordinates of the microscope stage at any predetermined number of positions.

This script was used to rapidly move the stage to different positions along a mesentery network as defined by the user. The script also controls the CCD camera (Coolsnap cf, Photometrics, Tucson, AZ) used to capture images of the microcirculation.

were marked. Before execution of the movement script, the ND 1.4 filter was inserted into a holder mounted such that the filter reduced the intensity of the laser light entering the rear of the microscope. The customized IPLab movement script was then executed, allowing each position to be saved in sequence. At each position, a 5 second Raman spectrum was taken, a velocity measurement, and a snapshot taken with the video attached to the computer that saved the recorded images. After all positions were captured, they were revisited and a new velocity and Raman spectra were recaptured. At the completion of the IPLab script, a series of snapshots encompassing the entire network was taken under the 20X objective. A blue filter was placed on the trans-illumination pathway to increase the contrast between the blood vessels and the interstitium to further aid subsequent image analysis.

Raman Spectrum Analysis

All spectra collected in both experiments were saved on a local computer. Each Raman spectrum was the cumulative signal of one exposure, with durations of 5, 10, 15, or 20 seconds. After conversion to ASCII format, they were exported into a customized software program designed specifically to streamline processing and estimate Hb O_2 saturation. Within the program, each spectrum was processed for the removal of cosmic ray spikes and normalized to a baseline level. No further processing was performed on the Raman spectra.

Using this custom program, an estimation of the Hb O_2 saturation was performed by comparing the peak ratios (PR) of the intensities of the resonance bands for

oxygenated (I_{oxy}) and deoxygenated (I_{deoxy}) hemoglobin. The following formula was used to calculate the peak ratio: $PR = I_{oxy}/(I_{oxy} + I_{deoxy}) \times 100$. I_{oxy} and I_{deoxy} were calculated by noting the absolute intensities at 1375 cm^{-1} and 1355 cm^{-1}, respectively. Hb O_2 saturation was then estimated as a percentage using the PR, according to the formula: Hb O_2 Sat = PR × a + b. The coefficients *a* (1.28 ± 0.018) and *b* (-6.39 ± 0.76) were obtained from calibration experiments in which Hb O_2 Sat was independently measured using the OSM3, adjusted for the animal's unique Hb absorption spectra. This methodology of Hb O_2 Sat calculation was originally outlined in a study by Torres Filho et al. (Torres Filho, Terner et al. 2005).

Image Analysis and Calculation of Microvascular Parameters

Extensive image analysis was required to evaluate the data collected during the *in vivo* experiments. The images of the points along the microvessel where Raman signals were collected, and the sequential snapshots of the complete microvascular network, were saved and exported to an image analysis program (Adobe Photoshop Elements 2.0, Adobe Systems, Inc., San Jose, CA).

Vessel Luminal Diameter Measurement

The diameter of arterioles and venules was measured in computerized digital images using the Coolsnap video camera and the 40X water immersion objective. A calibration was performed by recording the image of a stage micrometer (1 mm scale with one hundred marks at 10 μm intervals) at the same magnification as the video

microscopic recordings. All 40X images captured were then printed using the same print size as the 1 mm scale. A digital caliper was used to measure the distance between 5 marks of the scale. This allowed for the exact calculation of the ratio between a measured distance (mm) and length within the image (μm). Once this factor was established, the caliper was used to measure all diameters, once the print copies of all positions were obtained. These measured diameters (mm) were multiplied by the previously calculated factor to determine the true diameters (μm) at each position along the network.

Vessel Segment Length Measurement

Distance measurements between each position of the microvessel were also determined. Vessel segment length of arterioles and venules were measured using computerized image analysis of video sequences and a 20 X water immersion objective. The distance scale was also calibrated by recording the image of a stage micrometer at same magnification as the video microscopic recordings. For complete arteriolar and venular path lengths through a network, the cumulative lengths of the contiguous segments of the pathway were determined. Ten to fifteen images were captured using the 20X objective. Using Photoshop Elements, the individual images were combined into a photo mosaic to create a single image of each microvascular network and the data collection points were identified. Sketches of each network and the 40X snapshots of each position of measurement were used for this identification. Using the 20X mosaic, the distance between the first and last point of the microvessel was measured with a

digital caliper. These measured distances were divided by the previously calculated factor to determine the true distances between the measured positions along the network.

Blood Flow and Hb O_2 Saturation Gradient Measurement

Blood flow and Hb O_2 saturation were determined at each microvessel position. Blood flow (expressed in units of nl/sec) was calculated using the equation: $Q = V \times \pi \times D^2/4$, where V is the RBC velocity (in mm/sec), and D is the diameter in mm. The first step in determining Hb O_2 saturation gradients was to take the difference in Hb O_2 saturation between the first position of the vessel and the last position. The second step was to divide this number by the true distance between the points, as determined using the previously described procedure. Finally, each gradient was expressed as the average change in saturation per 100 μm of microvessel.

In vitro Protocol

The circulator was cleaned with a large volume of enzymatic cleaning solution and left to circulate for 5-10 minutes. During this time, heparin solution was created and the data acquisition software was calibrated to allow for sampling of the incoming gas mixture. After the cleaning solution was drained, the heparin solution was introduced and allowed to circulate for 5 minutes. Care was taken to ensure that this solution flushed through the sampling line and capillary tube. While the heparin solution was circulating, the mounting platform was transferred onto the stage of the Raman intravital microscope. The heparin solution was drained from the system and allowed to circulate

empty for several minutes to prevent dilution of the blood. After the blood was introduced into the system, the gas mixture was set to produce a relatively stable initial Hb O_2 saturation between 60% and 80%, as determined by the baseline sample measurement. The blood flow through the capillary tube was visualized using the 20X water immersion objective to align the axis of the velocimeter with that of blood flow. Axis alignment was performed by opening a live image on the computer and rotating the velocimeter. The initial RBC velocity was measured and reduced to 0.2 mm/sec. After checking to ensure that spectrometer aperture and light paths were set correctly, 2-3 Raman spectra were collected at each RBC velocity. This velocity was increased in increments as previously described, depending on the type of data being collected during that experiment day. Velocities were determined after adjusting the rotation speed of the peristaltic pump. After this adjustment, RBC velocity was constant during the acquisition of each set of Raman spectra. To create the filter conditions, the appropriate filter (ND 1.4 or 2.0) was inserted in the light path of the laser as it entered the rear of the microscope.

In vivo Protocol

Surgical procedure was performed as previous described. After the animal platform was transferred onto the microscope stage, the microvessels were visualized using the 20X water immersion objective. A detailed sketch of the primary branches of the network was drawn and labeled for direction of flow and positions to be captured. The objective was switched to the 40X water immersion objective and the image of network was brought into focus using the eyepiece. The network was observed under this magnification before the movement script was begun to verify that the preparation

was relatively motionless. A motionless prep assured that the laser spot stayed over the microvessel the entire length of the accumulation period. Additionally, the positions to be measured were assessed for adequate size, relative to the laser spot.

Once the network was assessed, the movement script was begun. At each position the data acquisition sequence was as follows:

1) The light path was established to the Coolsnap camera and the light intensity from the halogen lamp was increased to visualize the microvessel on the computer screen.
2) The image was brought into focus.
3) The axis of the velocimeter was aligned with the direction of blood flow by rotating the velocimeter head.
4) A snapshot of the vessel was obtained and immediately saved on computer.
5) After approximately 10-15 seconds of constant RBC velocity, a marker was created in the waveform. This marked the beginning of the 5 second section of the waveform that was analyzed for RBC velocity measurements.
6) The epi-illumination path for the laser was set up by switching the light path from the camera to the spectrometer.
7) The high pass filter was placed in the epi-illumination path, as was the 2 mm mirror necessary to direct the laser light on the preparation.
8) The laser light intensity was increased from zero.
9) The halogen light intensity was dimmed and fine adjustments to the stage were performed to move the laser spot precisely over the pre-determined position.

10) A five second accumulation was begun after the halogen light intensity was reduced to zero.

11) After saving the Raman spectrum, the laser intensity was reduced to zero

12) All changes made to prepare for epi-illumination were reversed so that the trans-illumination path was reestablished.

This procedure was repeated for each point along the network. After these points were saved, they were revisited for a second round of measurements. At this point, only RBC velocity and Raman spectra were acquired.

Statistical Analysis

Data from this study are presented as mean ± standard deviation except where noted. For correlation analysis, linear least-squares regressions were performed and the significance of the coefficient of determination was tested, with $p<0.05$ as the criterion for significance. The statistical significance between means of Raman calculated Hb O_2 Sat collected at a given RBC velocity with and without a filter was also determined. The statistical tests were performed using commercial computer software (Origin 7, OriginLab and Excel XP, Microsoft).

RESULTS

In vitro Experiments

Two separate experimental conditions were used to evaluate the possibility of photodamage in the hemoglobin molecule, as expressed as the difference between Raman Hb O_2 saturation and OSM3 Hb O_2 saturation. In the first condition, no neutral density filter was used to reduce the laser light intensity reaching the preparation. A total of 63 spectra were collected across an RBC velocity range of 0.1 – 1.4 mm/sec. Within this condition there were 3 groups of data collected under slightly different conditions. In the first no filter condition, 36 Raman spectra were collected within a velocity range of 0.2 – 1.4 mm/sec. The laser power was 0.85 mW at the level of the capillary tube. The accumulation time of the spectrometer was 5 seconds. The blood had a measured hematocrit of 20 % and the hemoglobin concentration (tHb) ranged between 8.0 and 10.5 g/dL (Table 1). In the second no filter condition, 14 Raman spectra were collected within a velocity range of 0.7 – 1.4 mm/sec. The laser power was at 0.67 mW and the accumulation time was 10 seconds (Table 3). The blood had a measured hematocrit of 40 % and the hemoglobin concentration ranged between 10 – 11 g/dL. In the third no filter condition, 10 Raman spectra were collected within an RBC velocity range of 0.1-0.6 mm/sec. The laser power was 0.76 mW at the level of the capillary tube. The accumulation time of the spectrometer was 5 seconds (Table 2). In the first two subconditions, there was a statistically significant negative correlation between RBC

velocity and the difference between Raman derived Hb O_2 saturation and the actual Hb O_2 Sat, as measured with the OSM3 (Figure 5 & Figure 6). In the third subcondition, there was no significant correlation between RBC velocity and Hb O_2 saturation difference. Within this condition, there was a significant difference between the mean of Hb O_2 saturation difference of Raman spectra collected at 0.2 mm/sec with no filter and the similar mean of spectra collected at the same RBC velocity with the ND 1.4 filter. This data is reported in Table 2. The statistical significance of all correlations was evaluated using regression analysis. The statistical difference between the means of Hb O_2 saturation difference at a given velocity with and without a filter was determined and summary of all data collected during the *in vitro* experiments is summarized in Table 3.

The second experimental condition involved the use of two neutral density filters to limit the blood exposure to the laser. The first filter reduced the light intensity by a factor of 1.4 and the second reduced the intensity by 2. Within this condition, 23 Raman spectra were collected within an RBC velocity range of 0.2 – 1.9 mm/sec. Four groups of data were collected within this filtered condition. In the first filter condition, 6 Raman spectra were collected with a ND 1.4 neutral density filter in place. The RBC velocity range was 0.2 – 0.6 mm/sec and the laser power at the level of the capillary tube was 0.67 mW. The accumulation time was 20 seconds. The blood had a measured hematocrit of 40 % and the hemoglobin concentration ranged between 10 and 11 g/dL (Table 4). The second filter condition was identical to the first except that a ND 2.0 filter was used instead of a ND 1.4. The measured velocity range was 0.21 to 1.8 mm/sec. Eight Raman

Table 1. RBC velocity and mean difference between Raman and corresponding OSM3 Hb O_2 saturation of all 5 second Raman spectra derived saturations

RBC Velocity (mm/sec)	n	Mean Hb O_2 Sat Difference (%)	S.D
0.2	3	39.0	4.0
0.3	5	35.4	3.4
0.4	4	27.3	5.6
0.5	4	23.5	1.3
0.6	4	20.3	2.1
0.7	4	21.5	2.5
0.8	3	14.5	1.0
0.9	2	11.4	0.6
1.2	3	10.5	1.4
1.4	4	14.8	5.3

Mean difference is expressed as the average difference between each Raman derived Hb O_2 saturation and the actual OSM3 derived Hb O_2 saturation for all Raman spectra taken at the specified velocity. The laser power at the level of the preparation is 0.85 mW. Standard deviation (S.D.) is given for the mean differences, and "n" is the number of Raman spectra taken at each velocity.

Table 2. RBC velocity and mean difference between Raman and corresponding OSM3 Hb O_2 saturation of 5 second Raman spectra derived Hb O_2 saturations.

RBC Velocity	n	Mean Hb O_2 Sat Difference (%)	S.D.
0.1	2	8.5	0.7
0.2	3	9.3	1.5
0.2 with ND 1.4 filter	3	1.7	0.6
0.3	2	11.0	4.2
0.6	3	11.0	1.0

Mean difference is expressed as the average difference between each Raman derived Hb O_2 saturation and the actual OSM3 derived Hb O_2 saturation for all Raman spectra taken at the specified velocity. The laser power at the level of the preparation was 0.76 mW. Standard deviation (S.D.) is given for the mean differences, and "n" is the number of Raman spectra taken at each velocity. Three spectra were taken at an RBC velocity 0.2 mm/sec with the ND 1.4 filter in place as a demonstration of the effect of a filter on the Raman derived Hb O_2 saturation.

Table 3. RBC velocity and mean difference between Raman and OSM3 Hb O_2 saturation for all 10 second Raman spectra derived Hb O_2 saturations taken.

RBC velocity (mm/sec)	n	Mean Hb O_2 Sat Difference (%)	S.D.
0.7	4	22.8	5.1
0.8	1	19.0	0
0.9	1	14.3	0
1.1	2	16.2	0
1.2	4	14.2	0.7
1.4	2	10.4	0

Mean difference is expressed as the average difference between each Raman derived Hb O_2 saturation and the actual OSM3 derived Hb O_2 saturation for all Raman spectra taken at the specified velocity without a neutral density filter. Standard deviation (S.D.) is given for the mean differences, and "n" is the number of Raman spectra taken at each velocity.

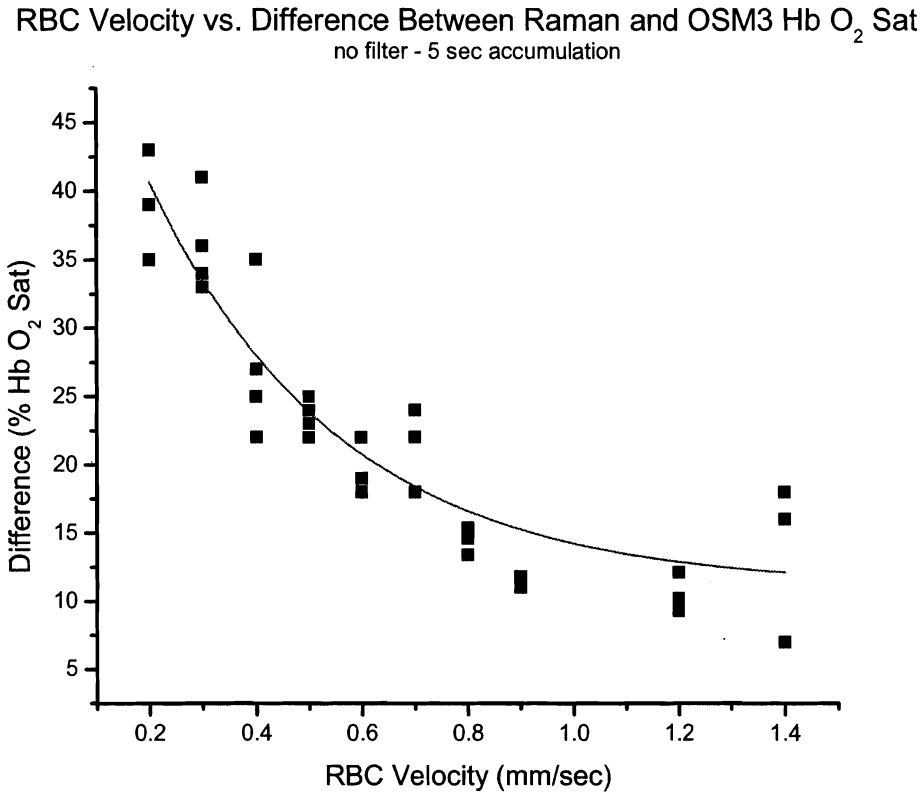

Figure 5. A scatter plot of data for RBC velocity versus the difference between Raman spectra derived Hb O_2 saturation and the corresponding OSM3 Hb O_2 saturation. The curve in the graph represents a best fit exponential decay of the data to the equation $y = 51.78e^{-x/0.36} + 11.06$. The correlation coefficient is -0.93, with $p<0.05$. The number of measurements is 32.

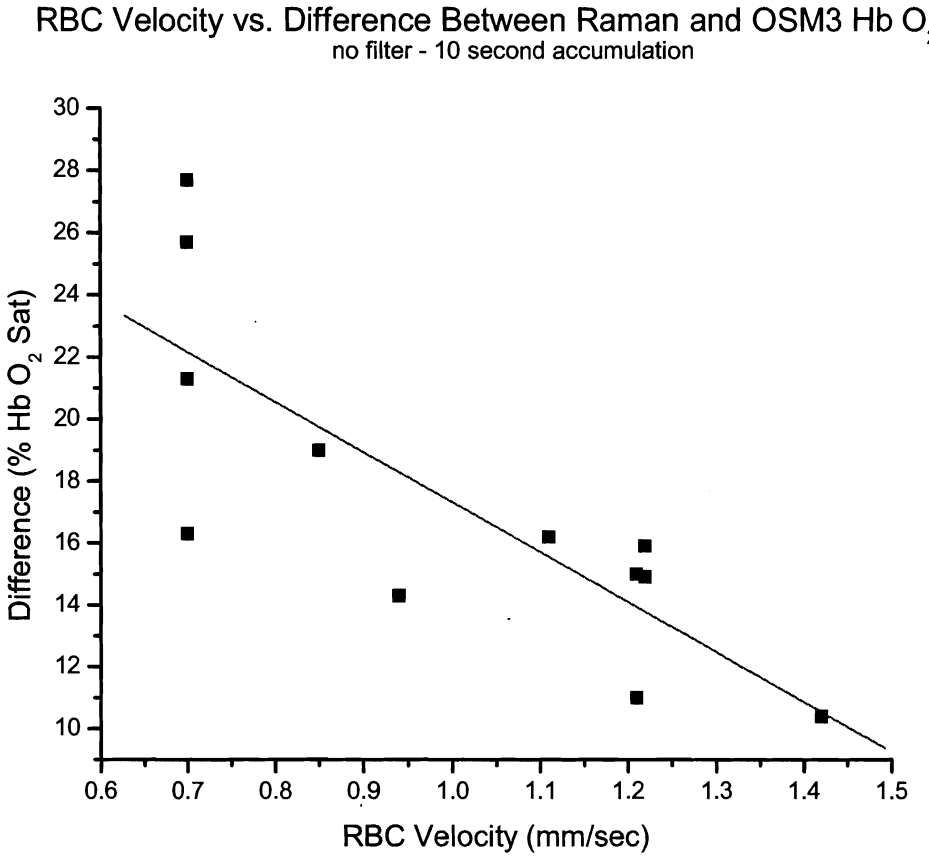

Figure 6. A scatter plot of data for RBC velocity versus the difference between Raman spectra derived Hb O_2 saturation and the corresponding OSM3 Hb O_2 saturation with no filter in place. The line in the graph represents a linear best fit of the data to the equation $y = -16.14x+33.47$. The correlation coefficient is -0.83, with $p<0.05$. The total number of measurements is 16.

Table 4. RBC velocity and mean difference between Raman and OSM3 Hb O_2 saturation for all 20 second Raman spectra derived Hb O_2 saturations taken.

RBC velocity (mm/sec)	n	Mean Hb O_2 Sat Difference (%)	S.D.
0.2	3	32.0	1.5
0.6	3	28.3	1.2

Mean difference is expressed as the difference between each Raman derived Hb O_2 saturation and the actual OSM3 derived Hb O_2 saturation for all Raman spectra taken at the specified velocity with the ND 1.4 filter in place. Standard deviation (S.D.) is given for the mean differences, and "n" is the number of Raman spectra taken at each velocity.

Table 5. RBC velocity and mean difference between Raman and OSM3 Hb O_2 saturation for all 20 second Raman spectra derived Hb O_2 saturations taken.

RBC velocity (mm/sec)	n	Mean Hb O_2 Sat Difference (%)	S.D.
0.2	2	34.8	2.1
0.6	3	23.7	7.8
1.8	3	11.6	2.1

Mean difference is expressed as the difference between each Raman derived Hb O_2 saturation and the actual OSM3 derived Hb O_2 saturation for all Raman spectra taken at the specified velocity with the ND 1.4 filter in place. Standard deviation (S.D.) is given for the mean differences, and "n" is the number of Raman spectra taken at each velocity.

spectra were collected within this subcondition (Table 5). In these filter conditions, a negative correlation was seen between RBC velocity and the difference between Raman derived Hb O_2 saturation and the OSM3 Hb O_2 saturation (Figures 7 & 8).

The last two filter conditions had identical tHb, hematocrit, and laser power as the previous two "filter" conditions. In both conditions, a ND 1.4 filter was used within the RBC velocity range of 0.9 – 1.9 mm/sec. The only difference was that in one filter condition, a ND 1.4 filter was used while in the other condition, the ND 2.0 filter was used. Four Raman spectra were collected at a 10 second accumulation time with the ND 1.4 filter and five spectra were collected at a 15 second accumulation time with the ND 2.0 filter. There was no statistically significant correlation between RBC velocity and difference between Raman and OSM3 derived Hb O_2 saturations. All data with a filter are summarized in Table 6.

In vivo Experiments

Seven microvascular networks were studied in 6 animals including a total of 8 arterioles and 7 venules. In some animals, more than one arteriole and venule was examined. All measured and calculated variables such as microvessel diameter, RBC velocity, blood flow, and Hb O_2 saturation were collected at each position twice per microvessel. In all microvessels, the total number of variables collected per microvessel varied depending if 2 or 3 positions were evaluated. The calculation of Hb O_2 saturation gradient required two points, thus, if two Hb O_2 saturation measurements could not be

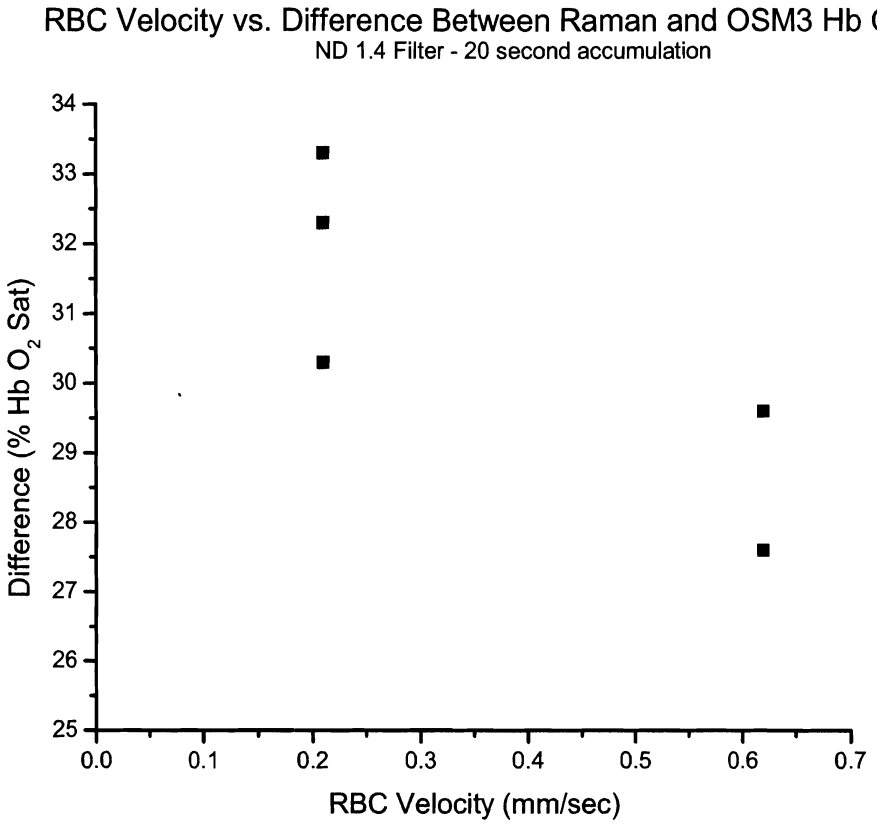

Figure 7. A scatter plot of data for RBC velocity versus the difference between Raman spectra derived Hb O_2 saturation and the corresponding OSM3 Hb O_2 saturation. The accumulation time for each Raman spectrum taken is 20 seconds.

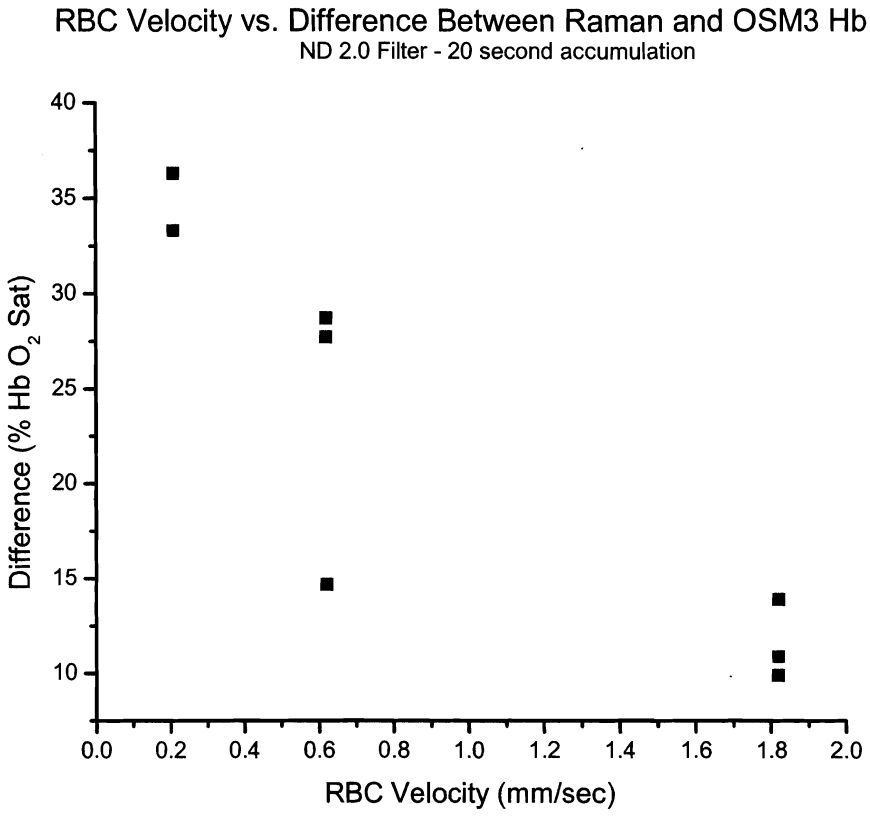

Figure 8. A scatter plot of data for RBC velocity versus the difference between Raman spectra derived Hb O_2 saturation and the corresponding OSM3 Hb O_2 saturation. The accumulation time for each Raman spectra taken is 20 seconds.

Table 6. A summary of all data collected during the *in vitro* experiments.

Filter used	N/A	N/A	N/A	1.4	2	1.4	1.4
RBC velocity (mm/sec)	0.2-1.4	0.7-1.4	0.1 - 0.6	0.2-0.6	0.2-1.8	0.9-1.8	0.9-1.9
Accumulation time (sec)	5	10	5	20	20	10	15
Laser power (mW)	0.85	0.67	0.76	0.48	0.34	0.48	0.48
Hematocrit (%)	20	40	28	40	40	40	40
tHb (g/dL)	8.0-10.5	10.0-11.0	8.5-10.0	10.0-11.0	10.0-11.0	10.0-11.0	10.0-11.0
Number of spectra collected within given RBC velocity range (n)	36	14	10	6	8	4	5

Each experimental condition is identified based on the presence of a neutral density filter, the velocity range the Raman spectra was collected within, and the accumulation time of the spectrometer. Measurements for hematocrit and hemoglobin concentration (tHb) were also collected. Hematocrit is expressed as a percentage. Hemoglobin concentration is given in g/dl. Laser power was measured at the level of the capillary tube.

taken along the length of a given microvessel in either round of data collection, an Hb O_2 saturation gradient could not be calculated. *In vivo* data were collected with the ND 1.4 filter with an accumulation time of 5 seconds. The laser power at the level of the preparation was 0.34 mW.

In 7 venules, data collection resulted in the generation of 40 individually measured values of diameter and 37 values of RBC velocity. Twenty seven values of Hb O_2 saturation were calculated and 8 could not be calculated due to excessive noise in the Raman spectra. Twelve Hb O_2 saturation gradients were calculated. Summary data for all venules are presented in Table 8. All comparisons performed between measured and calculated variables in all venules are presented in Table 11. There was a statistically significant negative correlation between RBC velocity and Hb O_2 saturation gradient (Figure 9). There was no significant correlation between blood flow and Hb O_2 saturation or between RBC velocity and Hb O_2 saturation.

In 8 arterioles, data collection resulted in the generation of 44 individually measured values of diameter and 41 values of RBC velocity. Thirty four values of Hb O_2 Sat were calculated and 5 could not be calculated due to excessive noise in the Raman spectra. There were three criteria for rejection: 1) A deoxy Hb peak height of below 30 (units of intensity); 2) a spectrum that could not be adjusted to accurately to baseline; and 3) any post analysis spectra that reported an Hb O_2 Sat over 100%. Twelve Hb O_2 Sat gradients were also calculated. Similar calculations were performed for the arterioles, as described above. Summary data for all arterioles are presented in Table 10. All comparisons performed between the measured and calculated variables in all arterioles are presented in Table 11. There was statistically significant negative correlation

between RBC velocity and Hb O_2 saturation gradient and between blood flow and Hb O_2 saturation gradient (Figures 10 & 11). There was no significant correlation found between RBC velocity and Hb O_2 saturation. Regression analysis was used to determine the statistical significance of all correlations in data collected in both arterioles and venules.

Table 7. A summary of the measurements made in 6 venules.

	Diameter		Velocity		Hb O_2 Sat		Hb O2 Sat Gradient	Blood Flow	
	(μm)	S.D.	(mm/sec)	S.D.	(%)	S.D.	%/100 μm	nl/sec	S.D.
venule 1a	18.2	0.6	0.66	0.07	74.0	8.5	**4.36**	0.16	0.01
venule 2	28.8	3.7	1.19	0.19	78.3	3.1	0.19	0.40	0.07
venule 2a	28.8	3.7	1.22	0.25	72.7	4.5	**0.48**	0.41	0.13
venule 4	24.5	9.3	0.83	0.16	83.5	5.0	0.84	0.24	0.06
venule 4a	24.5	9.3	0.80	0.23	78.7	3.1	0.47	0.20	0.03
venule 5	28.5	12.0	0.42	0.26	73.5	19.1	4.04	0.23	0.19
venule 6a	21.1	7.5	0.67	0.17	53.3	6.7	**1.71**	0.18	0.08
venule 7	30.9	3.3	1.30	0.45	52.3	6.1	0.58	0.61	0.14

Only venules in which all listed variables could be calculated are reported. The Hb O_2 saturation gradient describes the mean change in saturation from the first measured point along the vessel to the last measured point. Data in bold refers to saturations that *increased* as the blood moved downstream. All other gradients demonstrate that the saturation decreased as the blood moved downstream. Standard deviation (S.D.) is given for all means calculated. All labels with the "a" designation indicate a set of measurements that were the second of two taken in the same venule.

Table 8. A summary of the means for all measured and calculated measurements in all 7 venules.

	n	Mean	S.D.
Diameter (μm)	40	24.7	7.5
RBC Velocity (mm/sec)	37	0.7	0.4
Blood Flow (nl/sec)	37	0.3	0.2
Hb O_2 Sat (%)	27	68.4	12.4
Hb O_2 Sat Gradient (%/100 μm)	9	1.5	1.6

Standard deviation (S.D.) is given for all means, and "n" is the number of individual measurements included in the given mean.

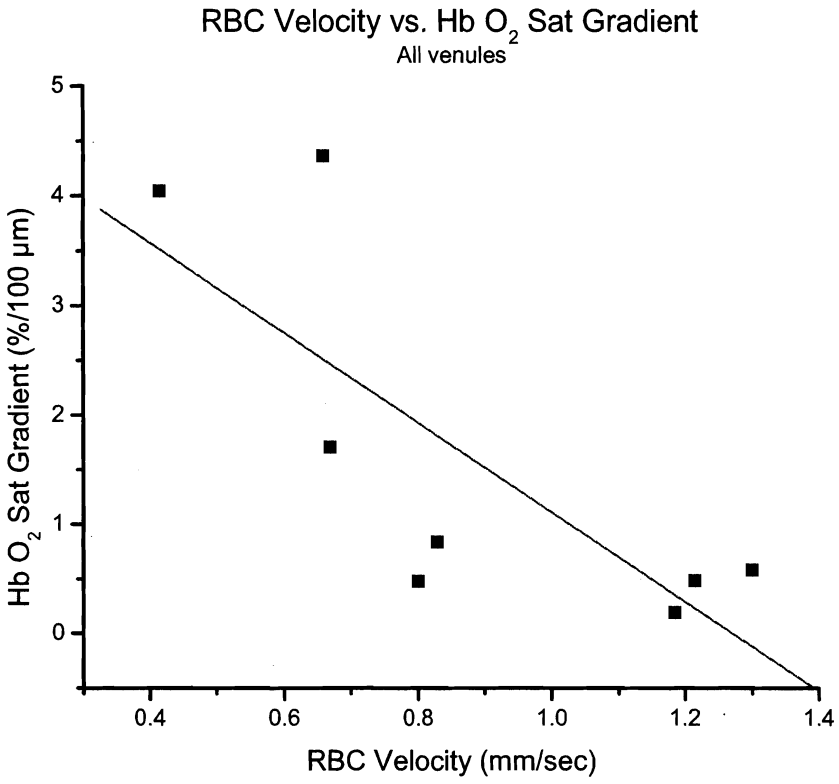

Figure 9. A scatter plot of the mean RBC velocity of a given venule versus the mean Hb O_2 saturation gradient in the same microvessel. The line in the graph represents a best fit exponential decay of the data to the equation $y = -4.10x + 5.21$. The correlation coefficient is -0.77, with $p<0.05$. The number of measurements is 9.

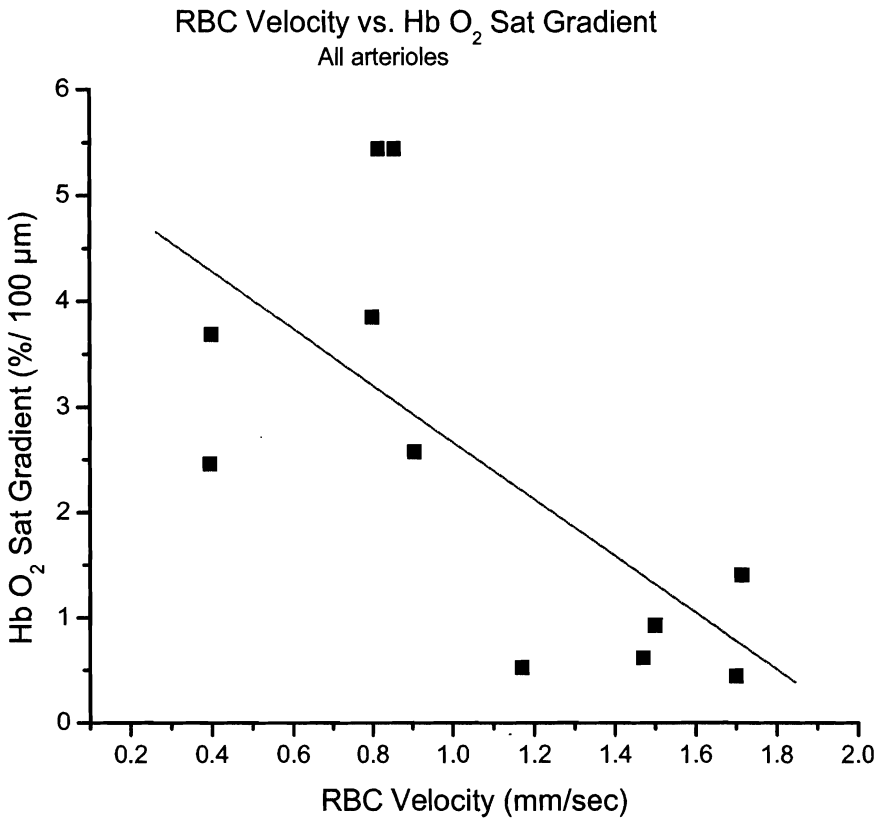

Figure 10. A scatter plot of the mean RBC velocity of a given arterioles versus the mean Hb O_2 saturation gradient in the same microvessel. The line in the graph represents a linear best fit of the data to the equation $y = -2.69x + 5.36$. The correlation coefficient is -0.69, with $p<0.05$. The number of measurements is 11.

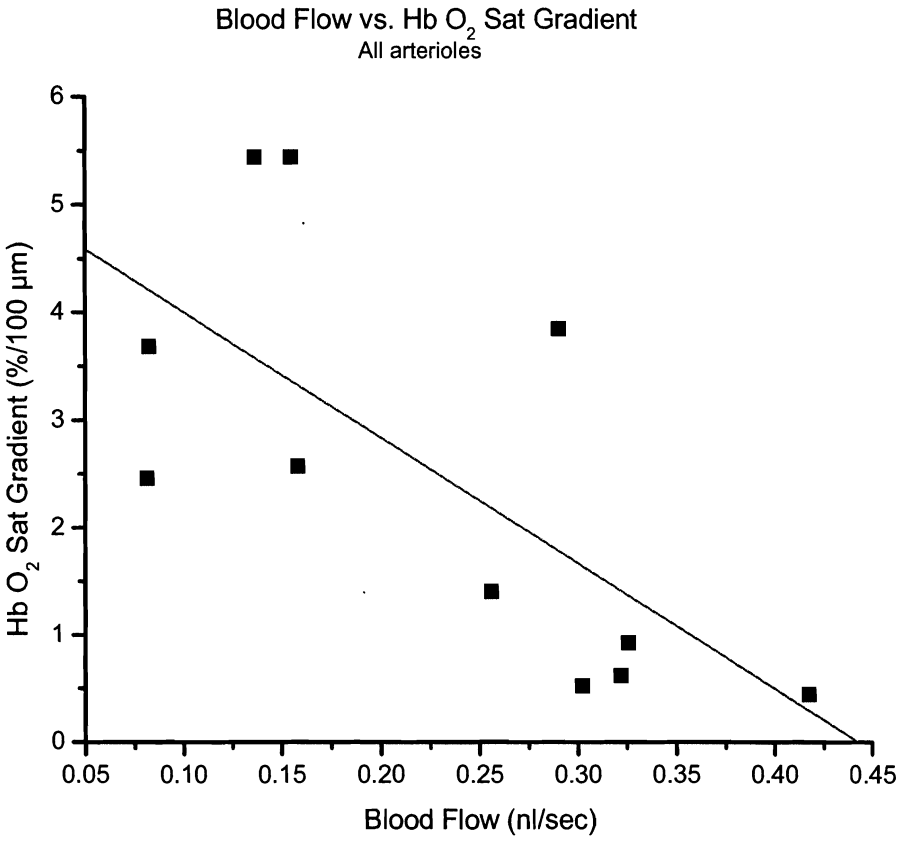

Figure 11. A scatter plot of the mean blood flow of a given arteriole versus the mean Hb O_2 saturation gradient in the same microvessel. The line in the graph represents a linear best fit of the data to the equation $y = -11.69x + 5.17$. The correlation coefficient is -0.69, with $p<0.05$. The number of measurements is 11.

Table 9. A summary of the measured and calculated measurements made in 8 arterioles.

	Diameter		Velocity		Hb O_2 Sat		Hb O_2 Sat Gradient	Blood Flow	
	(μm)	S.D.	(mm/sec)	S.D.	(%)	S.D.	%/100 μm	nl/sec	S.D.
arteriole 1	20.5	9.6	1.2	0.2	78.0	1.4	0.5	0.30	0.10
arteriole 2	17.2	2.0	1.5	0.1	67.3	6.5	0.6	0.32	0.05
arteriole 2a	17.2	2.0	1.5	0.2	74.0	5.2	**0.9**	0.33	0.06
arteriole 3	13.3	0.1	0.9	0.6	76.0	5.7	2.6	0.16	0.11
arteriole 4	15.9	2.7	0.4	0	82.5	6.4	3.7	0.08	0.02
arteriole 4a	15.9	2.7	0.4	0	79.0	4.2	2.5	0.08	0.02
arteriole 5a	13.3	3.1	1.7	0.5	74.7	14.2	**1.4**	0.26	0.09
arteriole 6	14.7	3.9	0.9	0.2	64.0	11.3	**5.4**	0.15	0.07
arteriole 6a	14.7	3.9	0.8	0.3	74.0	10.6	**5.4**	0.14	0.11
arteriole 7a	17.1	3.0	0.8	0.9	57.7	10.3	**3.8**	0.29	0.25
arteriole 8	16.0	1.5	1.7	0.6	65.3	1.5	**0.4**	0.42	0.12

Only arterioles in which all listed variables could be calculated are reported. The Hb O_2 saturation gradient describes the mean change in saturation from the first measured point along the vessel to the last measured point. Data in bold refers to saturations that *increased* as the blood moved downstream. All other gradients demonstrate that the saturation decreased as the blood moved downstream. Standard deviations (S.D.) are given for all means calculated. All labels with the "a" designation indicate a set of measurements that were the second of two taken in the same arteriole.

Table 10. A summary of the mean for measured and calculated measurements in 8 arterioles.

	n	Mean	S.D.
Diameter (μm)	44	15.9	3.6
RBC Velocity (mm/sec)	41	1.3	0.7
Blood Flow (nl/sec)	41	0.3	0.2
Hb O_2 Sat (%)	34	70.9	9.5
Hb O_2 Sat Gradient (%/100 μm)	12	2.3	1.9

Standard deviation (S.D.) is given for all means, and "n" is the number of individual measurements included in the given mean.

Table 11. A summary of all comparisons performed between measured and calculated variables in all microvessels.

	Variable		Correlation Coefficient (r)	N	Significant Correlation
Venules	Diameter	Gradient	-0.53	9	No
	Diameter	Saturation	0.30	12	No
	Velocity	Saturation	0	12	No
	Velocity	Gradient	-0.77	9	Yes, $p<0.03$
	Flow	Gradient	-0.57	9	No
	Flow	Saturation	-0.10	12	No
Arterioles	Diameter	Gradient	-0.48	11	No
	Diameter	Saturation	0.20	15	No
	Velocity	Saturation	-0.42	15	No
	Velocity	Gradient	-0.69	11	Yes, $p<0.03$
	Flow	Gradient	-0.69	11	Yes, $p<0.02$
	Flow	Saturation	-0.47	15	No

Comparisons were performed between the listed variables for all arterioles and venules in which a complete set of measurements and calculations could be performed. The correlation coefficient was calculated using the best linear fit line of the data. The presence of a significant correlation was calculated using regression analysis. All significant r values are reported with the degree of significance. "N" refers to the number of mean calculations of each variable included in the comparison.

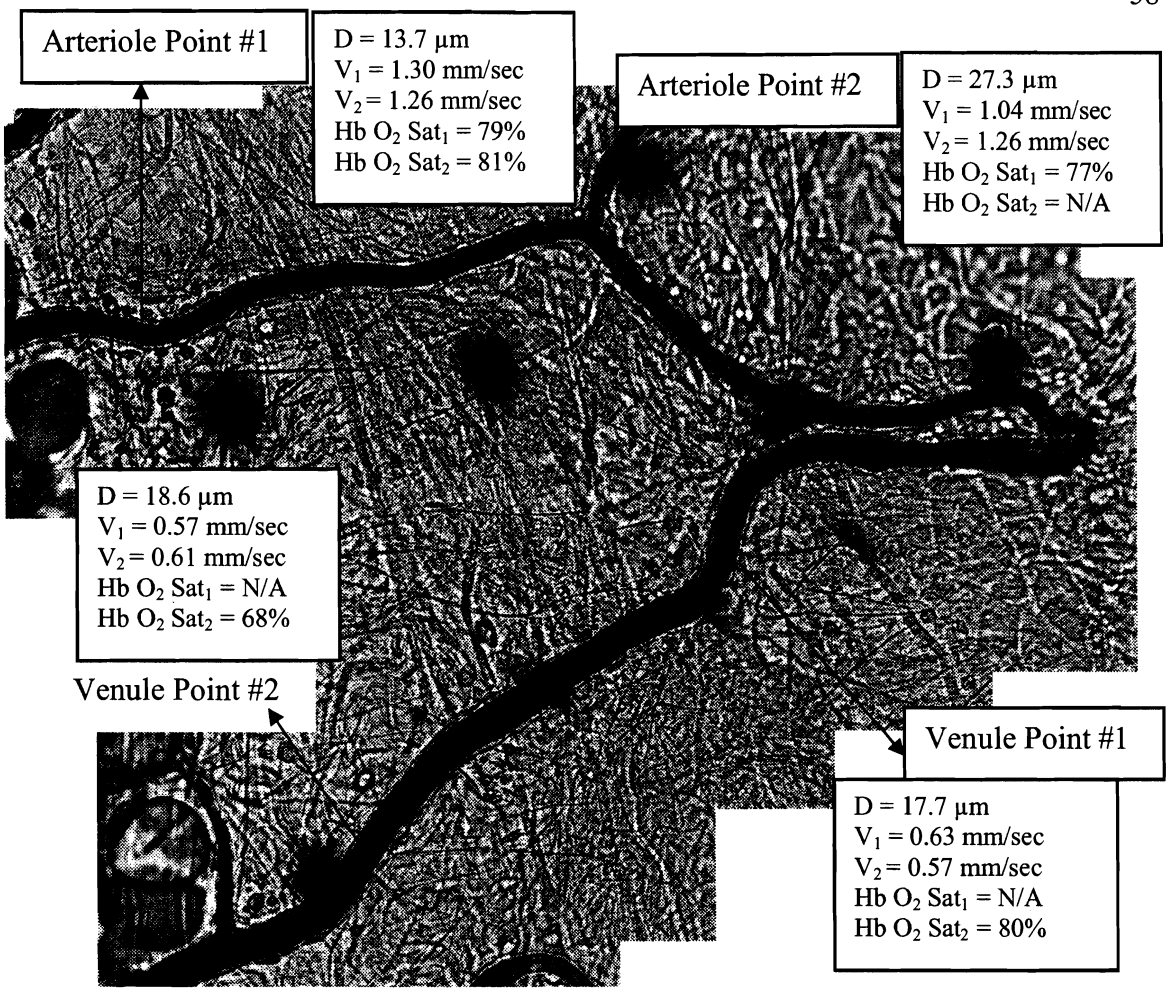

Figure 12. Image is a mosaic of 18 separate screen captures of a single mesentery network using the 20X water immersion objective. Raman spectra, RBC velocity and diameter, measured at 40X magnification, were captured at all identified points. The arteriolar measurements were collected in sequence (#1 then #2), followed by the venular points. All points were revisited in a second set of measurements through the network where RBC velocity and Raman spectra were captured. Measured length between arteriolar and venular points was 380 µm and 275 µm, respectively. Final magnification is 223X.

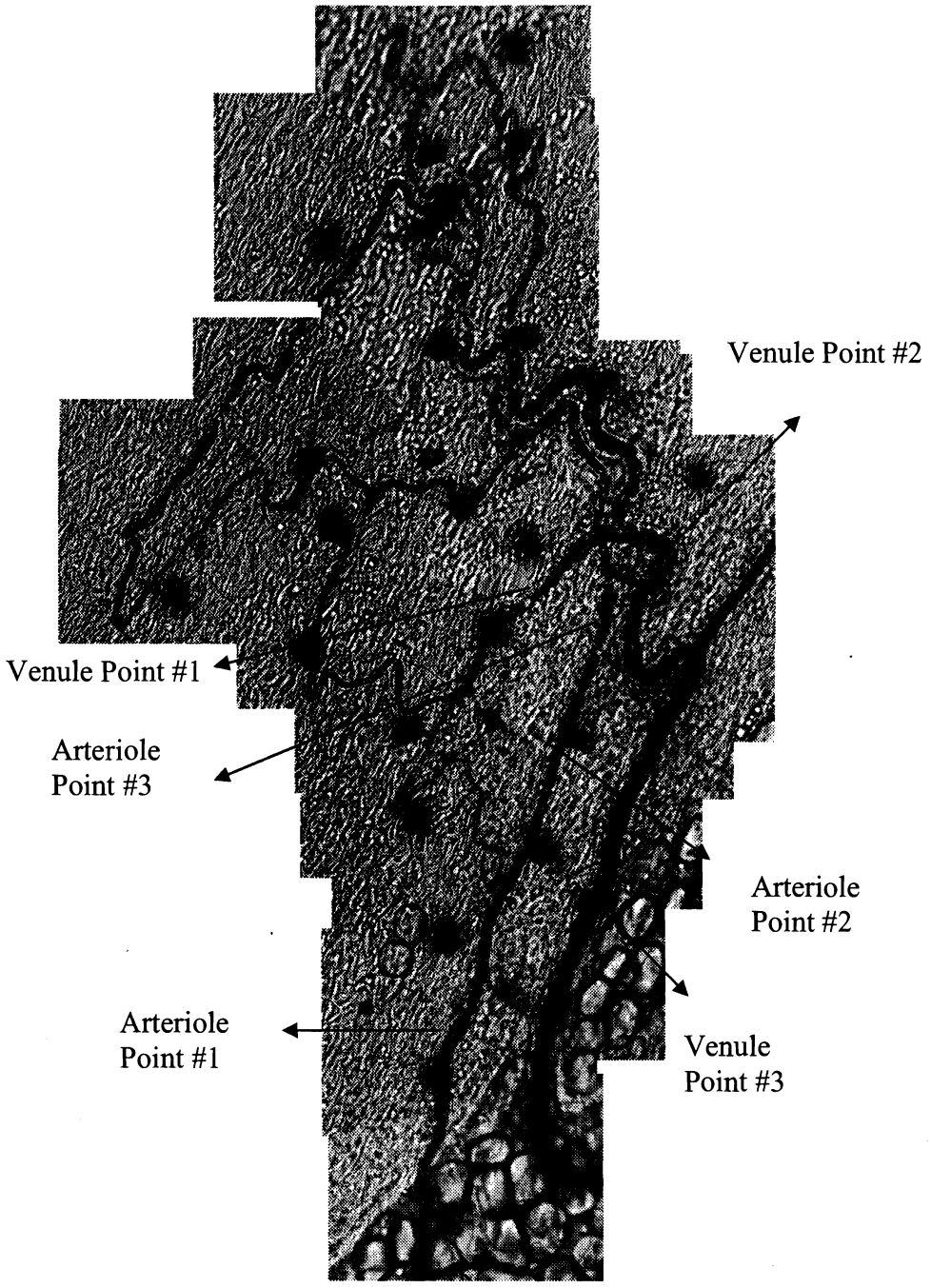

Figure 13. Image is a mosaic of 30 screen captures of a microcirculatory network using the 20X objective. Final magnification is 113X. Sequence in measurement identical to Figure 12.

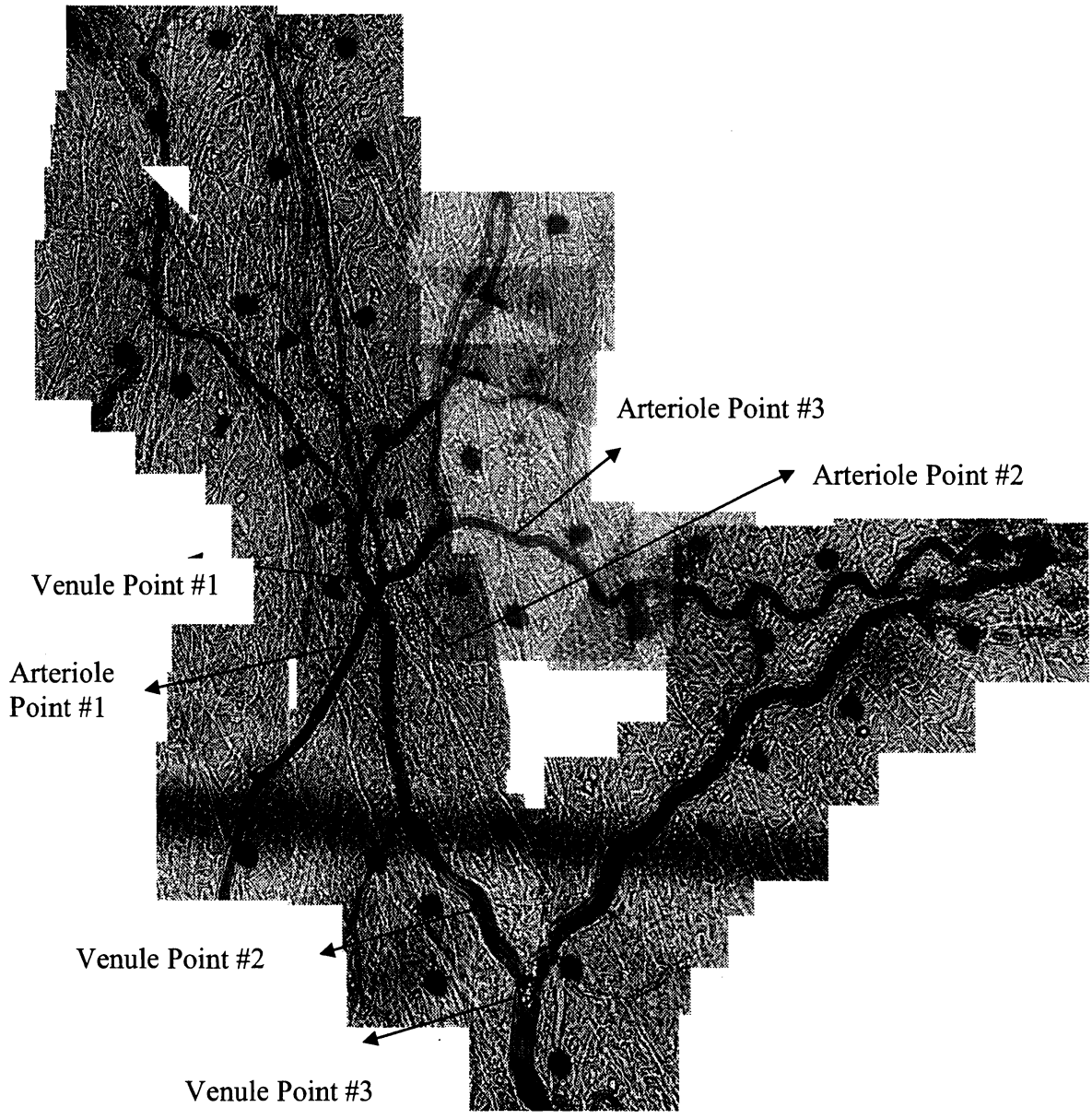

Figure 14. Image is a mosaic of 50 screen captures of a single mesentery microcirculatory network using the 20X water immersion objective. Final magnification is 100X. Sequence in measurement identical to Figure 12.

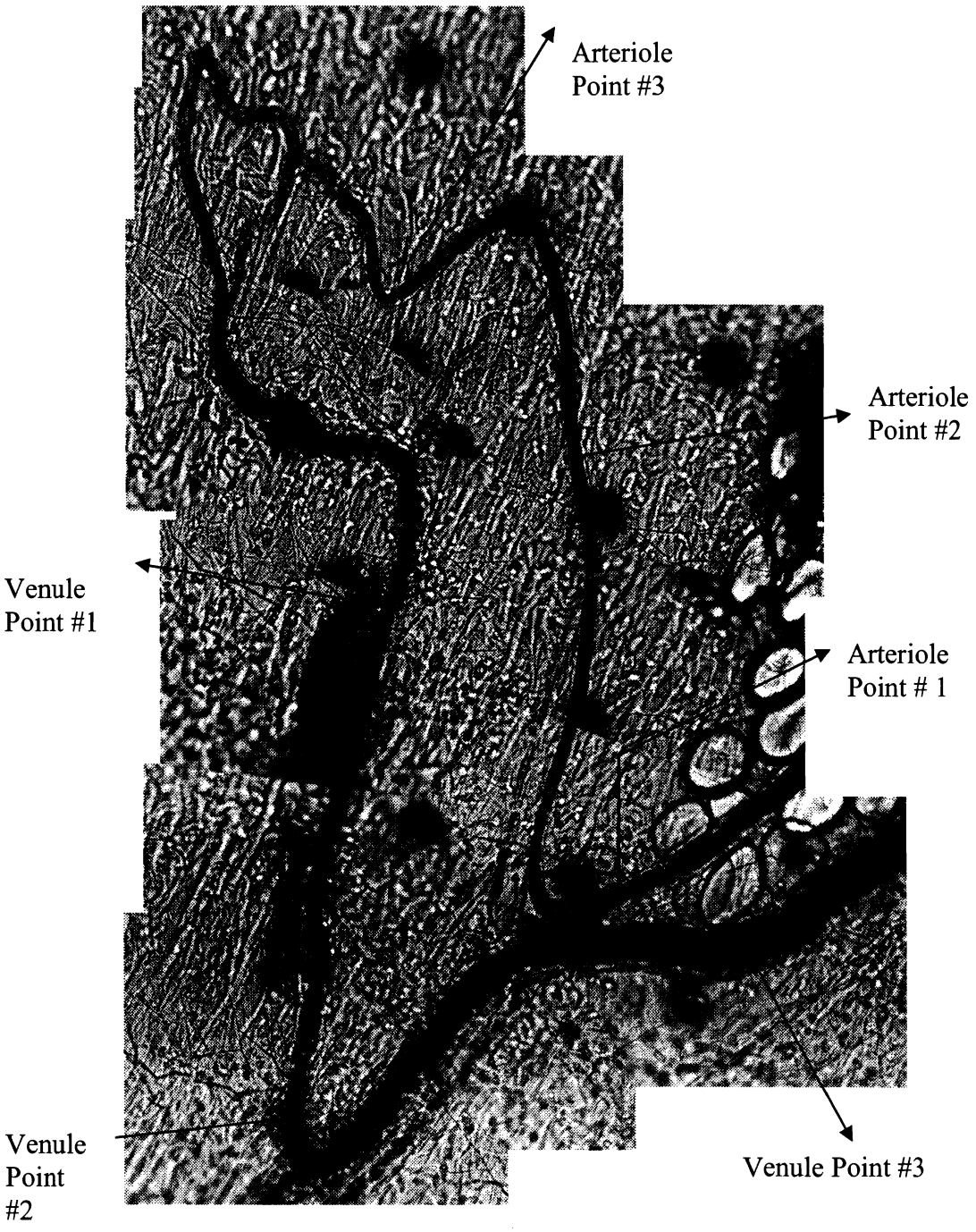

Figure 15. Image is a mosaic of 15 screen captures of a single mesentery microcirculatory network using the 20X water immersion objective. Final magnification is 202X. Sequence in measurement identical to Figure 12.

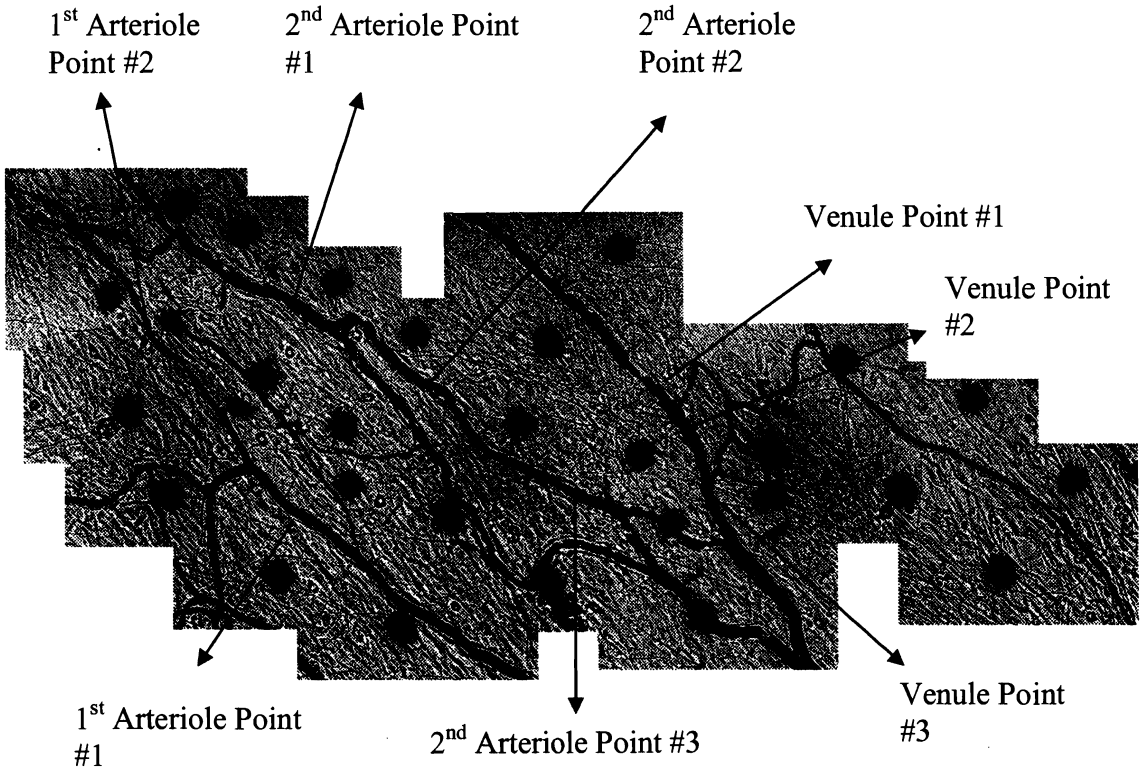

Figure 16. Image is a mosaic of over 18 screen captures of a single mesentery microcirculatory network using the 20X water immersion objective. Final magnification is 132X. Sequence in measurement identical to Figure 12

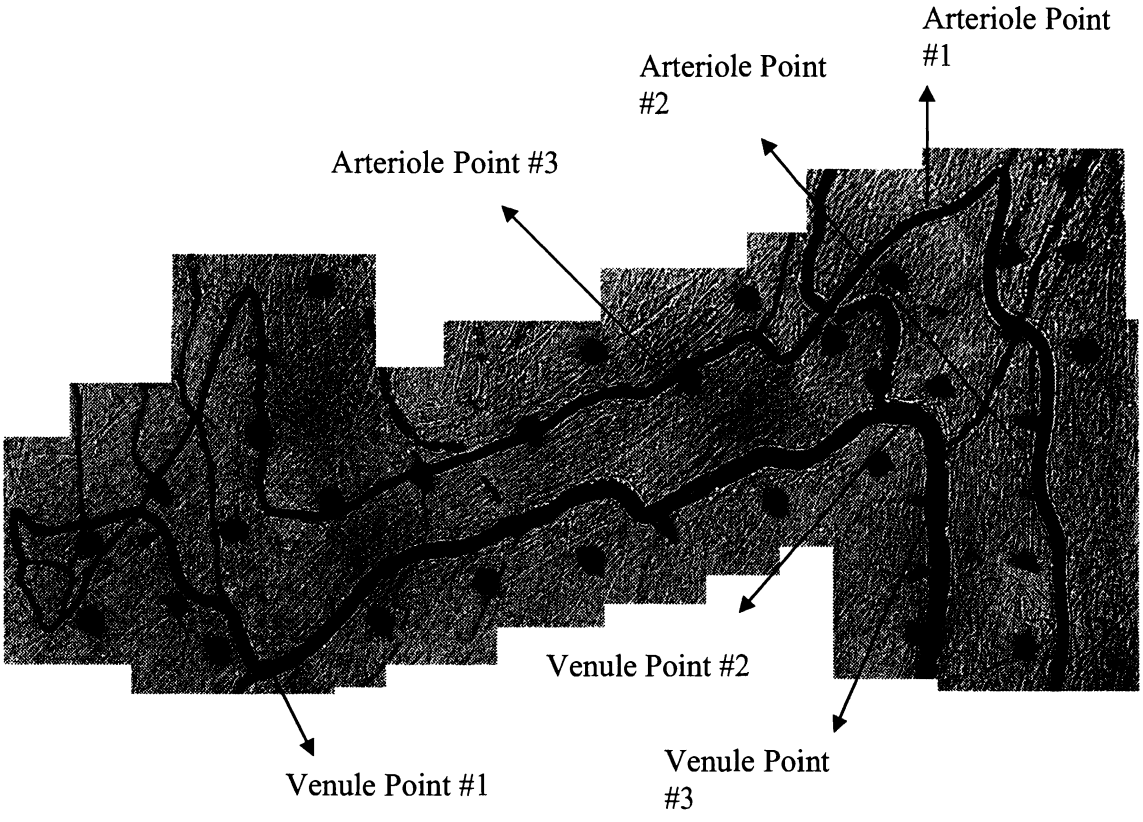

Figure 17. Image is a mosaic of 31 screen captures of a single mesentery microcirculatory network using the 20X water immersion objective. Final magnification is 83X. Sequence in measurement identical to Figure 12.

DISCUSSION

The purpose of this study was to utilize an *in vitro* system to further characterize the photodegradative effect on hemoglobin caused by utilizing Raman spectroscopy on slowly moving blood. With a better understanding of this effect, more precise Hb O_2 saturation measurements can be made at a wide variety of RBC velocities. The second part of this study was to use this knowledge to test the efficiency of a stage movement system to rapidly and accurately determine the presence of Hb O_2 saturation gradients in the blood. Any possible gradient changes were examined in arterioles and venules for a relationship with the RBC velocity.

Importance of RBC Velocity

Previous Raman studies have examined the state of oxy-hemoglobin in single red blood cells under constant laser power (between 0.7 and 2.0 mW). They noted that there is a transition to deoxy-hemoglobin using various laser wavelengths, particularly at 488 and 514 nm (Nollmann and Etchegoin 2000; Ramser, Bjerneld et al. 2003). Wavelengths of approximately 720 nm have clearly shown RR spectra of the heme moieties with little interference with fluorescence or presence of O_2 photodissociation under constant laser illumination at 1-2 minute exposure times. (Puppels, Olminkhof et al. 1991; Sato, Chiba

et al. 2001). The most obvious trend when examining these studies is that lower wavelength excitation light caused severe dissociation of O_2 from the hemoglobin molecule due primarily to photodamage. The degree of photodamage could be quantified by observing the transition of oxy-hemoglobin to deoxy-hemoglobin. Additionally, it should be stated that many of these experiments generated Raman spectra using accumulation times that were on the order of minutes using a laser power range of 0.75 - 20 mW.

In this study, an *in vitro* circulator was used to circulate blood through a resonance Raman intravital spectroscopy system so that RBC velocity and hemoglobin oxygen saturation measurements could be made. Since a 406 nm laser was used in this study, it was expected that even very low accumulation times (10-20 sec) and low laser power (less than 1 mW) would create photodissociation of oxygen from hemoglobin in unmoving whole blood. This effect was observed in this study and that of Torres Filho et al (2005). It was hypothesized that the accumulated photon dose of the hemoglobin was the major determinant of the extent of photodamage in the molecule. In order to evaluate different exposure times of red blood cells to the laser light during acquisition of a Raman spectrum, whole blood was circulated through an *in vitro* system at varying RBC velocities. Photodamage of the hemoglobin molecule was quantified by observing the difference between the Raman Hb O_2 saturation and OSM3 Hb O_2 saturation. In this study, this difference was calculated as the RBC velocity was gradually increased. There was a statistically significant negative correlation between the RBC velocity and the difference between Raman Hb O_2 saturation and OSM3 Hb O_2 saturation. Tests performed with 5 and 10 second accumulation times indicated that increased RBC

velocity at a constant laser power reduced the absolute difference between the two calculated Hb O_2 saturations.

We hypothesized that the power of the excitation light and the RBC velocity were the biggest factors in the determination of the extent of photodamage and photodissociation of O_2 from oxy-hemoglobin. The power of the excitation laser was important because it directly determined how much total energy per time a given red blood cell would absorb as it flowed past the laser spot. The RBC velocity was important because it determined how long the cells were under the laser illumination. In order to reduce the extent of photodamage to hemoglobin, RR spectra must be collected in conditions of reduced laser power on the flowing blood and a RBC velocity high enough so that RBC exposure to the laser light is minimal. The *in vitro* results suggested that in experimental conditions where Hb O_2 saturation was held constant, decreasing the total laser energy over a given RBC cell decreased the extent of photodamage, regardless of the accumulation time (Figures 18 & 19).

The relationship between RBC velocity and total energy on a single RBC at the three power levels used in the *in vitro* experiments is given in Table 13. As expected, it is apparent that at higher RBC velocities, the total laser energy on a single RBC decreased due to the decrease in exposure time. The energy absorbed by a given RBC in flowing blood is a function of both RBC velocity and laser power. Photodamage and photodissociation of O_2 in hemoglobin are primarily due to these factors. Increasing the accumulation time will simply increase the number of RBC's under the laser, not the

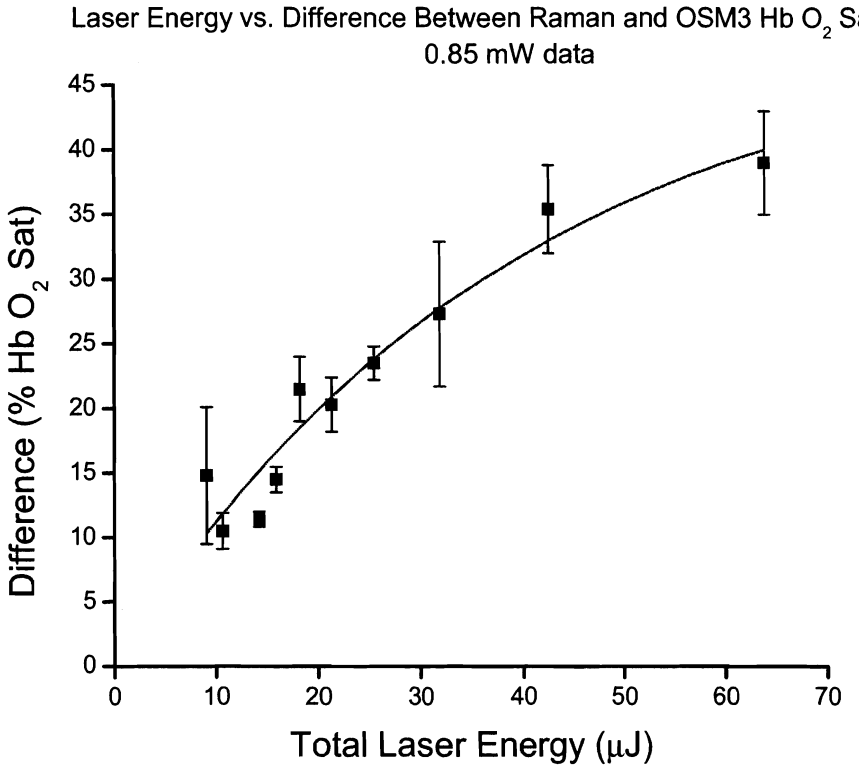

Figure 18. A scatter plot of the estimated total energy absorption of a single RBC versus the mean difference between Raman spectra derived Hb O_2 saturation and the corresponding OSM3 Hb O_2 saturation. Data used in this plot was collected using RR spectra collected at a laser power of 0.85 mW and accumulation time of 5 seconds. The energy absorbed by a single RBC was estimated by calculating the length of time it took an RBC to cross the laser illumination spot of a diameter of 15 μm at the RBC velocities used in the given *in vitro* experimental condition. All other aspects of the experimental condition were kept constant except the RBC velocity. The line in the graph represents an exponential best fit of the data. The correlation coefficient is 0.96, with $p<0.05$. Vertical bars indicate the standard error of the mean.

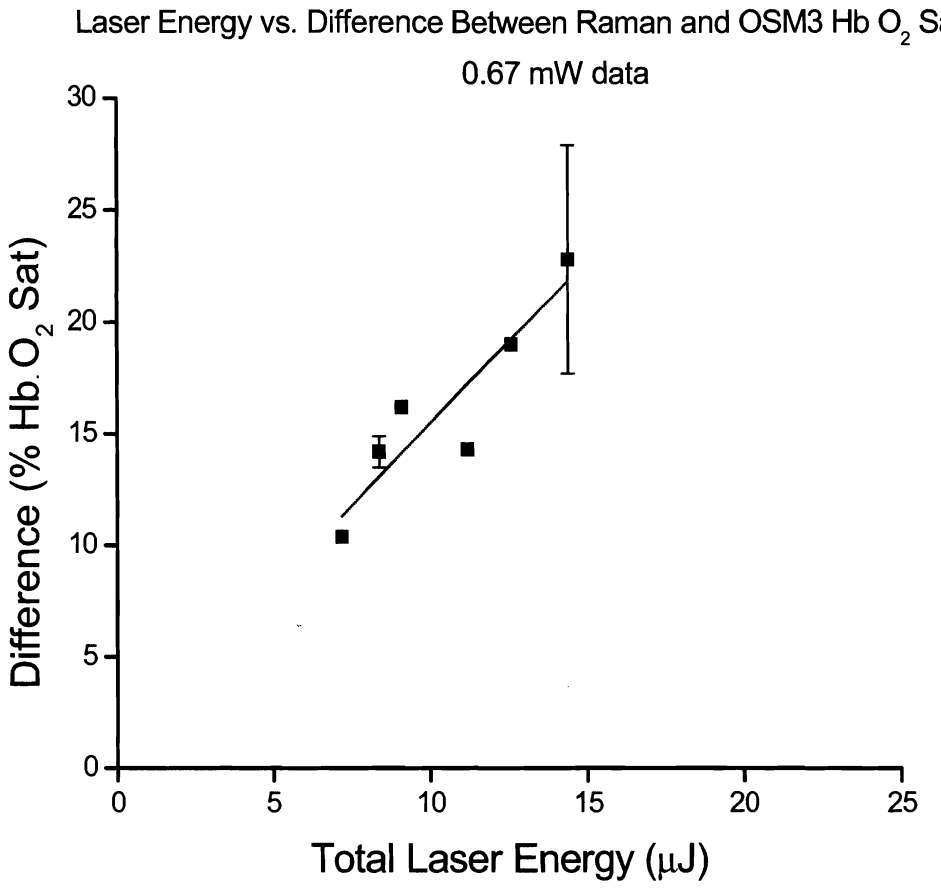

Figure 19. A scatter plot of the estimated total energy absorption of a single RBC versus the mean difference between Raman spectra derived Hb O_2 saturation and the corresponding OSM3 Hb O_2 saturation. Data used in this plot was collected using RR spectra collected at a laser power of 0.67 mW and accumulation time of 10 seconds. The method of calculating the energy absorbed by a single RBC was identical to Figure 18. All other aspects of the experimental condition were kept constant except the RBC velocity. The line in the graph represents a linear best fit of the data. The correlation coefficient is 0.91, with $p<0.05$. Vertical bars indicate the standard error of the mean.

Table 12. Comparison of the total laser energy exposure of a single RBC moving at the given velocity across an excitation laser spot of 15 μm.

RBC Velocity (mm/sec)	Total Laser Energy at 0.85 mW (μJ)	Total Laser Energy at 0.76 mW (μJ)	Total Laser Energy at 0.67 mW (μJ)	Total Laser Energy at 0.34 mW (μJ)
0.1	127.5	114.0	100.5	51.0
0.2	63.8	57.0	50.3	25.5
0.3	42.5	38.0	33.5	17.0
0.4	31.9	28.5	25.1	12.8
0.5	25.5	22.8	20.1	10.2
0.6	21.3	19.0	16.8	8.5
0.7	18.2	16.3	14.4	7.3
0.8	15.9	14.3	12.6	6.4
0.9	14.2	12.7	11.2	5.7
1.0	12.8	11.4	10.1	5.1
1.1	11.6	10.4	9.1	4.6
1.2	10.6	9.5	8.4	4.3
1.3	9.8	8.8	7.7	3.9
1.4	9.1	8.1	7.2	3.6
1.5	8.5	7.6	6.7	3.4
1.6	8.0	7.1	6.3	3.2
1.7	7.5	6.7	5.9	3.0
1.8	7.1	6.3	5.6	2.8
1.9	6.7	6.0	5.3	2.7
2.0	6.4	5.7	5.0	2.6

All calculations were performed using an average RBC diameter of 6 μm. The approximate laser energy exposure is provided at the laser power in the various experimental conditions in which statistically significant data was gathered.

length of exposure time over individual cell. In this study, photodamage of the hemoglobin molecule could be characterized by a change of oxy-Hb to deoxy-Hb.

Several RR spectra were collected under identical conditions except for the presence of a neutral density filter that reduced the laser power by a factor of 1.4 at the level of the microscope stage. The mean difference in calculated Hb O_2 saturation of three spectra collected with a ND 1.4 filter, at an RBC velocity of 0.2 mm/sec, was determined to be statistically different from the mean difference in calculated Hb O_2 saturation of three spectra collected with no filter at the same velocity. It appears that the filter condition was able to reduce the difference between the two calculated Hb O_2 saturation values to less than 2 %. Based on this finding, the *in vivo* data were collected using 5 second accumulation times and the ND 1.4 filter. In order to assure that virtually no photo-effects were introduced into the *in vivo* data collection procedure, all RR spectra taken during this procedure were collected at an incident laser power of 0.34 mW. At this laser power and accumulation time, it was believed that the laser exposure would allow us to collect RR spectra with RBC velocities as low as 0.3 - 0.4 mm/sec without risk of significant Hb O_2 photodissociation.

In vivo Experiments

There were two main goals of the *in vivo* experiments. The first was to determine how quickly microvascular measurements could be made using resonance Raman spectroscopy. A custom designed stage movement script was created that allowed positions, as defined by the user, to be saved and moved to rapidly in sequence.

However, it was unknown until this study, how rapidly microcirculatory parameters could be measured. The second goal was to use this system, regardless of the speed of data acquisition, to determine the presence of Hb O_2 saturation gradients in the arterioles and venules of microcirculatory networks using resonance Raman spectroscopy.

In order to collect several microvascular parameters to conduct the *in vivo* studies, it was important to know how fast the acquisition could be performed. The Raman intravital microscope used in this experiment was uniquely designed such that two illumination paths, epi- and trans-illumination, could be easily utilized. Switching between the two pathways could be done quickly (within seconds) with no effect on the mesentery preparation. Hemoglobin oxygen saturation measurements using resonance Raman scattering were made using the epi-illumination pathway while RBC velocity and diameter measurements used trans-illumination. Since the RBC velocity and images used to measure microvessel luminal diameter were gathered optically, there was no interference with the preparation. Several other studies have similarly utilized intravital microscopy to make accurate *in vivo* measurements of variables such as RBC velocity, blood flow, hematocrit, and hemoglobin oxygen saturation (Toth, Tischler et al. 1992; Pal, Toth et al. 1993; Torres Filho, Terner et al. 2005).

There are few studies that have adapted a computer controlled stage for rapid data acquisition within the *in vivo* framework. The programmable stage interface program used in this study was similar to that used by (Pal, Toth et al. 1993). The user was able to input the positions in the microvasculature where data collection was to take place. The computer saved these positions and could revisit them indefinitely if needed. In the current study, additional control over stage was added so that the program paused

between each position to allow for data collection of parameters that were not automated such as velocity and Raman spectrum acquisition. The program was designed to proceed to the next position only if instructed by the user. This program increased the speed of data acquisition along the entire network.

Factors Influencing Rapid Data Collection

In vivo measurements, such as resonance Raman acquisition and RBC velocity, could be collected with this system as rapidly as 30-45 seconds, with approximately 1-4 minutes between each Raman spectra. In this ideal situation, two complete rounds of microvascular measurements could be taken within 20 minutes. However, when *in vivo* data was first collected, it took 20-40 minutes between shots, for a total of nearly 1.5 hours to collect data from the entire network. As was expected, increased efficiency in later experiments allowed all other mesenteries to be measured within 45 minutes in their entirety.

The ideal data collection procedure required 3 very important situations to occur. First, it was vital that positions chosen were of the same orientation to reduce the need to align the axis of the velocimeter with that of blood flow. It could take up to 1-2 minutes to focus the computer image and align the velocimeter with the axis of blood flow at the new position. Secondly, the preparation needed to be still, especially during Raman acquisition. Peristalsis, a mesentery positioned improperly, or an animal's breathing could move the preparation slightly. All of these conditions needed to be controlled. Since these experiments were performed in live animals, it was not always possible to

keep the preparation from moving slightly. Often, a few seconds of peristalsis was enough to move the laser spot off the vessel and into interstitial space. If this occurred during Raman acquisition, the result was an unusable spectrum. The inability to obtain well defined spectra could easily add minutes between Raman acquisitions.

Another aspect of data collection that could increase time spent was the need to manually switch between the computers and various instruments needed to collect data via epi- and trans-illumination. The snapshots needed for diameter measurements and RBC velocity measurements needed to be collected using the trans-illumination pathway and Raman spectra required the epi-illumination pathway. As detailed previously, many elements of this transition could not be automated, which prevented more rapid data acquisition.

In vivo Findings

Due to the fact that O_2 delivery to tissue is primarily accomplished by diffusion, a time limited process, it follows that circumstances that reduce the time for this process in microvessels should decrease difference in the Hb O_2 Sat from one end of a microvessel to the other end. This difference was expressed in the current study as the rate of change in Hb O_2 Sat per 100 μm of microvessel, otherwise known as the Hb O_2 Sat gradient. There was a statistically significant negative correlation between mean RBC velocity and Hb O_2 saturation gradient in both arterioles and venules. We found that in both arterioles and venules, higher RBC velocities were associated with reduced Hb O_2 Sat gradients. This effect was present whether the hemoglobin oxygen saturation was increasing or

decreasing downstream. Other studies that have examined longitudinal hemoglobin oxygen saturation gradients in skeletal muscle have found significantly higher gradients along the length of 4^{th} order or terminal arterioles than those found in this study (Swain and Pittman 1989). Work by Itoh et al (Itoh, Yaegashi et al. 1994) in the rat mesentery, revealed that the average PO_2 decreased as blood moved downstream in an arteriole. Although in this study the statistical significance of the findings was not explored, observation of the presented data clearly showed a distinct change in the oxygen distribution depending if the animal was breathing 100% O_2 or room air. No gradients could be observed under anoxia conditions but 100% O_2 conditions brought about obvious radial and longitudinal gradients. Analysis of PO_2 gradients have shown a marked decrease in oxygen content as blood moves through from the primary arterioles to the terminal arterioles. However, within an individual vessel, it has been shown that these gradients are very small, approximately 0.3 mmHg/100 μm (Torres Filho, Kerger et al. 1996). An estimation of this gradient expressed in terms of hemoglobin oxygen saturation was 0.34 %/100 μm. The average arteriolar Hb O_2 Sat gradient in arterioles for our study was 2.61 ± 1.76 %/100 μm, a value that is higher than that found in the previously described study and the 1.8 %/100μm calculated in the study of Swain and Pittman (1989). An estimation of the mean PO_2 gradient in our study was 9.4 ± 8.1 mmHg/100 μm using an algebraic rearrangement of the known equation of the hemoglobin O_2 dissociation curve for rat blood (Lowman 2004):

$$\text{Hb } O_2 \text{ Sat} = 100^* (PO_2)^{2.7} / (36^{2.7} + (PO_2)^{2.7}).$$

Venular Hb O_2 Sat has been found to increase sequentially moving from the terminal venules to the first order venules (Swain and Pittman 1989; Shonat and Johnson

1997). Although only the terminal venules were examined in this study, an Hb O_2 Sat gradient was seen in several of these microvessels. The average Hb O_2 Sat gradient in all venules was 1.5 ± 1.6 %/100 μm (or an estimated PO_2 gradient of 7.64 ± 7.82 mmHg/100 μm), a gradient that was not found to be statistically different from that of arterioles.

There was also a significant negative correlation between blood flow and Hb O_2 saturation gradient in arterioles. The *in vivo* data suggested that increasing the blood flow reduced the mean Hb O_2 saturation gradient of a given microvessel. This is not a surprising finding considering that velocity and flow are interrelated. This effect was not demonstrated in venules despite a very strong correlation between mean venular RBC velocity and Hb O_2 Sat gradient. However, there was a trend in the data that suggested that a similar correlation between the two parameters exists. It appears that more data points would be needed to confirm this.

Limitations and Future Studies

Although several trends in the data have been elucidated, additional study is warranted. The results of the *in vitro* studies indicate that more data points are needed to more precisely determine the minimum energy exposure (as measured using RBC velocity) needed to greatly reduce the difference in calculated Hb O_2 saturation using resonance Raman spectroscopy and the OSM3. It was difficult to collect data at RBC velocities greater than 1.9 mm/sec because of the increase in pressure within the system. Fluid leakage caused at least one *in vitro* experiment to be prematurely aborted. The data suggested that increases in RBC velocity over 2.0 mm/sec would further decrease the

degree of photodamage, but more data would need to be collected at these higher velocities to support this hypothesis.

The large amount of *in vitro* data collected under identical conditions suggests a non-linear relationship between calculated Hb O_2 saturation and RBC velocity. However, a significant percentage of the data was collected below 1 mm/sec, so future studies should explore this relationship at RBC velocities between 1 and 2.5 mm/sec. It is unknown if this relationship is truly non-linear or linear.

Two observations can be made upon examination of all the data. First, the microvascular parameters within arterioles and venules changed very rapidly at times, in the order of minutes. There were points along the same microvessel that had virtually identical Hb O_2 saturations (<5% difference) after both rounds of measurements, but had a point 400 μm downstream with Hb O_2 saturations (after two rounds of measurements) that differed by over 15%. This was typical in approximately half the microvessels examined. Due to the speed at which microvascular parameters changed within the vessels under observation, the current data acquisition set up did not allow for a high degree of temporal sensitivity. Under the ideal conditions, the precise size of an Hb O_2 Sat gradient should be measured by taking optical measurements simultaneously at two different positions along the microvessel to account for this temporal variability. However, we believe that the correlation between Hb O_2 gradients and RBC velocity was not significantly affected by this temporal variability in Hb O_2 Sat due to the speed at which each RBC velocity and Hb O_2 Sat was taken at the positions along the microvessel (<5 – 10 seconds). The average time for the evaluation of a given microvessel was approximately 15-20 minutes. Secondly, a comparison of the average Hb O_2 saturation

in venules and arterioles revealed only a 2% decrease across the capillaries. This may support previous studies that have shown small PO_2 gradients between terminal arterioles and venules (Torres Filho, Terner et al. 2005).

Exploration of *in vivo* data might involve further optimization of the data collection procedure to reduce the time spent outside of data collection. Improvements to the signal processing might allow for noisier Raman spectra to be analyzed. As mentioned previously, some spectra were analyzed by the program incorrectly so that some of the peaks could not be distinguished from the background fluorescence. Future modifications of the custom signal analysis tool should allow for weaker signals to be processed accurately.

Another modification that should help signal interpretation would be to allow for further cooling of the CCD camera. For various mechanical reasons, the cooling unit within the camera did not allow to it to be cooled past -41.5 °C. Reducing thermal noise by using lower cooling temperatures could affect spectra acquisition. If additional cooling allowed weaker Raman signals to be processed, it would be possible to use a lower laser power to induce the Raman scattering or perhaps shorten the acquisition time to 1 or 2 seconds, reducing the possibility of photodamage even more.

Another interesting idea to improve data processing would be to allow for real time signal processing. The possibility of real time acquisition, background correction, and smoothing has been explored in a Raman system designed to collect *in vivo* data (Bakker-Schut 2002). In this study, several interfacing programs were installed on the computer where the Raman spectra were saved. The setup used by the authors was one that allowed them to make calculations on Raman spectra collected within seconds. The

authors speculated that with further optimization of the software and computer, processing of Raman spectra could be reduced by a factor of five. This would allow for an analysis of real time RR spectra along the order of milliseconds. In the current study, data analysis of all data was performed off-line. The ability to perform real time calculations of hemoglobin oxygen saturation while collecting the raw spectra would allow the user to tailor data acquisition from moment to moment. Additional ideas for automation can be found in a study by Toth et. al ((Toth, Tischler et al. 1992) who were able to set up a system that could collect data for NADH fluorescence, Hb O_2 Sat (using the 3 wavelength method), hematocrit, tissue PO_2, and other microcirculatory variables virtually simultaneously. Automation of all the optical paths was required for this to occur. It might be possible to automate several aspects of our own Raman microscopy system, including the transition between epi and illumination paths as well as switching between various filters. This might allow us to shorten data acquisition times so that entire networks could be captured in minutes for virtually real time analysis of longitudinal hemoglobin oxygen saturation gradients.

Summary and Conclusions

In vitro studies of the effect of red blood cell velocity on the accuracy of Hb O_2 Sat measurements using RR spectroscopy have demonstrated that increasing the speed of the blood increases the accuracy of these measurements by reducing the amount of time that an individual RBC is exposed to the laser light. By reducing the length of time that a given oxygenated hemoglobin molecule is exposed to the energy of the excitation laser,

the degree of photodamage is reduced significantly. Photodamage was characterized by the difference between Raman and OSM3 derived Hb O_2 Sat values and described the presence of the deoxygenated form of hemoglobin in an environment where it would normally be oxygenated. This photodamage will manifest in a photo-induced dissociation of O_2 from oxy-hemoglobin, converting it to deoxy-Hb. An examination of the average energy exposure of each RBC at a given velocity revealed that in order to significantly reduce the degree of photodamage, an RBC must not be exposed to greater than 10 μJ of laser energy as it moves across the excitation spot. This threshold was the point at which there was an approximate 10% difference between the two methods of measuring Hb O_2 Sat. Additionally, increasing the laser exposure of an RBC, by experimentally reducing the RBC velocity, resulted in an increase in photodamage.

The *in vitro* experiments determined what the approximate minimal laser energy, and the corresponding RBC velocity, to which flowing blood should be exposed to most accurately measure Hb O_2 Sat gradients using RR spectroscopy. The *in vivo* experiments allowed for the accurate RR measurement of Hb O_2 Sat gradients using a computer-controlled stage movement system. Acquisition of several microvascular parameters taken at 2-3 positions along selected arterioles and venules could be accomplished in under 10-15 minutes using this system. The effect of red blood cell velocity on the presence of Hb O_2 Sat gradients was also experimentally evaluated in arterioles and venules. As blood flowed downstream these microvessels, increased red blood cell velocity was associated with smaller hemoglobin oxygen saturation gradients *in vivo*.

REFERENCES

Bakker-Schut, T. C. W., Rolf; Caspers, Peter J., & Puppels, Gerwin. J. (2002). "Real-time tissue characterization on the bass of in vivo Raman spectra." Journal of Raman Spectroscopy **33**: 580-585.

Borders, J. L. and H. J. Granger (1984). "An optical doppler intravital velocimeter." Microvasc Res **27**(1): 117-27.

Davis, M. J. (1987). "Determination of volumetric flow in capillary tubes using an optical Doppler velocimeter." Microvasc Res **34**(2): 223-30.

Duling, B. R. and R. M. Berne (1970). "Longitudinal gradients in periarteriolar oxygen tension. A possible mechanism for the participation of oxygen in local regulation of blood flow." Circ Res **27**(5): 669-78.

Golub, A. S. and R. N. Pittman (2003). "Thermostatic animal platform for intravital microscopy of thin tissues." Microvasc Res **66**(3): 213-7.

Hanlon, E. B., R. Manoharan, et al. (2000). "Prospects for in vivo Raman spectroscopy." Phys Med Biol **45**(2): R1-59.

Intaglietta, M., P. C. Johnson, et al. (1996). "Microvascular and tissue oxygen distribution." Cardiovasc Res **32**(4): 632-43.

Itoh, T., K. Yaegashi, et al. (1994). "In vivo visualization of oxygen transport in microvascular network." Am J Physiol **267**(5 Pt 2): H2068-78.

Ivanov, K. P., A. N. Derry, et al. (1982). "Direct measurements of oxygen tension at the surface of arterioles, capillaries and venules of the cerebral cortex." Pflugers Arch **393**(1): 118-20.

Kobayashi, H. and N. Takizawa (2002). "Imaging of oxygen transfer among microvessels of rat cremaster muscle." Circulation **105**(14): 1713-9.

Krough, A. (1959). The anatomy and physiology of capillaries. New York, Hafner Publications.

Levy, M. N. (2004). Overview of the Heart, Blood Vessels, and Blood. Physiology. R. M. L. Berne, Matthew N, Elsevier, Inc: 265-273.

Levy, M. N. (2004). Oxygen and Carbon Dioxide Transport. Physiology. R. M. L. Berne, Matthew N, Elsevier, Inc: 498-510.

Lowman, J. D. J. (2004). Effects of emphysema and chronic hypoxemia on skeletal muscle oxygen supply and demand. Physiology. Richmond, Virginia Commonwealth University: 62-63.

Nollmann, M. and P. Etchegoin (2000). "Photoinduced oxygen dynamics in lyophilized hemoglobin." Spectrochim Acta A Mol Biomol Spectrosc **56**(14): 2817-29.

Pal, M., A. Toth, et al. (1993). "A computer controlled system for multiple site microcirculatory measurements." Microvasc Res **45**(1): 95-105.

Pittman, R. N. (1986). "In vivo photometric analysis of hemoglobin." Ann Biomed Eng **14**(2): 119-37.

Pittman, R. N. (1998). The Microcirculation and Tissue Oxygenation. Update in Intensive Car Medicine.

Pittman, R. N. and B. R. Duling (1975). "A new method for the measurement of percent oxyhemoglobin." J Appl Physiol **38**(2): 315-20.

Puppels, G. J., J. H. Olminkhof, et al. (1991). "Laser irradiation and Raman spectroscopy of single living cells and chromosomes: sample degradation occurs with 514.5 nm but not with 660 nm laser light." Exp Cell Res **195**(2): 361-7.

Ramser, K., E. J. Bjerneld, et al. (2003). Importance of substrate and photo-induced effects in Raman spectroscopy of single functional erythrocytes. J Biomed Opt. **8:** 173-8.

Ramser, K., K. Logg, et al. (2004). "Resonance Raman spectroscopy of optically trapped functional erythrocytes." J Biomed Opt **9**(3): 593-600.

Sato, H., H. Chiba, et al. (2001). "Excitation wavelength-dependent changes in Raman spectra of whole blood and hemoglobin: comparison of the spectra with 514.5-, 720-, and 1064-nm excitation." J Biomed Opt **6**(3): 366-70.

Shonat, R. D. and P. C. Johnson (1997). "Oxygen tension gradients and heterogeneity in venous microcirculation: a phosphorescence quenching study." Am J Physiol **272**(5 Pt 2): H2233-40.

Spiro, T. G. (1974). "Resonance Raman Spectroscopy: a New Structure Probe for Biological Chromophores."

Spiro, T. G. and R. S. Czernuszewicz (1995). "Resonance Raman spectroscopy of metalloproteins." Methods Enzymol **246**: 416-60.

Spiro, T. G. and T. C. Strekas (1974). "Resonance Raman spectra of heme proteins. Effects of oxidation and spin state." J Am Chem Soc **96**(2): 338-45.

Swain, D. P. and R. N. Pittman (1989). "Oxygen exchange in the microcirculation of hamster retractor muscle." Am J Physiol **256**(1 Pt 2): H247-55.

Torres Filho, I. P., H. Kerger, et al. (1996). "pO2 measurements in arteriolar networks." Microvasc Res **51**(2): 202-12.

Torres Filho, I. P., J. Terner, et al. (2005). "Hemoglobin oxygen saturation measurements using resonance Raman intravital microscopy." Am J Physiol Heart Circ Physiol **289**(1): H488-95.

Toth, A., M. E. Tischler, et al. (1992). "A multipurpose instrument for quantitative intravital microscopy." J Appl Physiol **73**(1): 296-306.

Tsai, A. G., P. C. Johnson, et al. (2003). "Oxygen gradients in the microcirculation." Physiol Rev **83**(3): 933-63.

Wang, Y. and H. E. Van Wart (1993). "Raman and resonance Raman spectroscopy." Methods Enzymol **226**: 319-73.

Wood, B. R., McNaughton, Don (2002). "Micro-Raman characterisation of high and low-spin moieties within single living erythrocytes." Biopolymers Biospectroscopy **67**: 259-262.

Wood, B. R., McNaughton, Don (2002). "Raman excitation wavelength investigation of single red blood cells in vivo." Journal of Raman Spectroscopy **33**: 517-523.

Wood, B. R., B. Tait, et al. (2001). "Micro-Raman characterisation of the R to T state transition of haemoglobin within a single living erythrocyte." Biochim Biophys Acta **1539**(1-2): 58-70.

VITA

Derrick V. Williams was born on January 11, 1979 in Alexandria, Virginia and is a citizen of the United States. He graduated high school from Thomas Jefferson High School for Science and Technology in Alexandria, Virginia in 1997. He received a Bachelor of Science in Psychology in 2001 from James Madison University in Harrisonburg, Virginia. He subsequently enrolled in the Physiology Certificate Program at Virginia Commonwealth University in 2003. Following completion of the program in 2004, he entered the Masters of Science program in physiology, which he completed in 2005. He will be starting medical school in fall of 2005.